applied sciences

MDPI

Article

Mechanism and Empirical Study of Rockburst in the Adjacent Area of a Fully Mechanized Top-Coal Caving Face Based on Microseismic Technology

Quanjie Zhu [1], Longkun Sui [2], Yongming Yin [3,*], Jinhai Liu [1], Zhenhua Ouyang [2] and Dacang Wang [2]

[1] School of Emergency Technology and Management, North China Institute of Science and Technology, Langfang 065201, China; youyicun2008@163.com (Q.Z.)
[2] School of Mine Safety, North China Institute of Science and Technology, Langfang 065201, China; slkyyds@163.com (L.S.)
[3] China Academy of Safety Science and Technology, Beijing 100012, China
* Correspondence: yinyongming@126.com

Abstract: Monitoring and providing warnings for coal mine rockburst disasters is a worldwide problem. Several rockburst accidents have occurred in a 1301 belt transport chute near a 1300 fully mechanized caving mine face. To address this issue, an empirical study of the occurrence mechanism of rockbursts in the adjacent area of the fully mechanized top-coal caving face was carried out. This paper mainly addresses the following issues: (1) based on microseismic monitoring technology, the distribution characteristics of the host-rock-supported pressure of the 1300 working face were measured, and the evolution and distribution of the deep-well caving working face host-rock-supported pressure were analyzed. It is revealed that the occurrence mechanism of rockburst in the adjacent area is actually caused by the evolution and superposition of the lateral abutment pressure of the 1300 stope, and the stress of the original rock along the 1301 belt transport down chute; (2) a theoretical calculation model of dynamic and static abutment pressure in longwall stope is built, and an example is tested. The results show that the peak position of lateral abutment pressure of the coal body outside the 1300 goaf is around 63 m, and the peak value of abutment pressure is around 47 MPa; (3) coal body stress monitoring, bolt dynamometer detection, and other means are compared and analyzed. At the same time, with the help of CT geophysical prospecting and drilling cutting measurements, it is concluded that the 1301 belt transport down chute is in the bearing pressure influence zone (superimposed zone), which further verifies the validity of microseismic analysis results and the accuracy of the above theoretical model. Based on this, the early warning system and prevention measures for rockburst based on microseismic monitoring are proposed. The engineering practice shows that the dynamic and static bearing pressure distribution and evolution law of the working face can be dynamically obtained by using microseismic technology, which provides a basis for the accurate prediction and treatment of rockbursts.

Keywords: rockburst; bearing pressure; microseismic technology; mining influence; actual measurement verification

Citation: Zhu, Q.; Sui, L.; Yin, Y.; Liu, J.; Ouyang, Z.; Wang, D. Mechanism and Empirical Study of Rockburst in the Adjacent Area of a Fully Mechanized Top-Coal Caving Face Based on Microseismic Technology. *Appl. Sci.* **2023**, *13*, 6317. https://doi.org/10.3390/app13106317

Academic Editor: Tiago Miranda

Received: 2 April 2023
Revised: 18 May 2023
Accepted: 18 May 2023
Published: 22 May 2023

1. Introduction

China is the country most severely threatened by dynamic disasters such as rockburst worldwide. According to statistics, the number of deaths caused by rockburst accidents in coal mines has shown a decreasing trend in the past decade. However, the occurrence of rockburst accidents in coal mines still presents an upward trend. The reason for this is that with the depletion of shallow coal resources in China, coal mining is characterized by an increasing mining depth, more extensive underground excavation, and more frequent coal pillar mining. This leads to increasing difficulties in coal mining and frequent occurrences of dynamic disaster accidents [1–4]. In addition, compared to China, other

countries may experience fewer rockburst accidents, but the resulting damages and associated mine disasters, such as roof fall and roof caving in longwall mining faces, should not be overlooked [5]. It is evident that deep coal mine dynamic disasters, including rockbursts, have become a major issue faced by the mining industry, seriously restricting the safe and efficient production of enterprises both domestically and abroad [6–10]. In response to this issue, experts from around the world have conducted extensive research on the distribution and evolution of support pressure in comprehensive coal mining faces, and have made some progress in understanding the occurrence mechanism, monitoring, early warning, and prevention of rockbursts [9,11–16].

The distribution of support pressure is the key factor to determine the stability of the working face and ensure the safety of miners. The evolution of the support pressure distribution is affected by many factors, such as the geological structure of the coal seam, the excavation method, the properties of the roof and floor strata, geological fault zones, and the type of filling wall [17,18]. Generally, as the work faces the deep coal seam, the support pressure tends to increase due to the increase in the weight of the overlying strata. Continuous monitoring and analysis of the distribution of support pressure is of great significance to predict and prevent the potential failure or collapse of the working face [19,20]. Advanced numerical simulation technology, such as finite element analysis, can be used to simulate and understand the distribution of support pressure and its evolution with time, as well as to establish effective models of fractured rock masses to improve execution speed [21–24]. Ansys software (https://www.ansys.com/ Last accessed date: 8 May 2023) can also be utilized to simulate the stress environment of the surrounding rock in a roadway under different filling wall conditions, and subsequently choose the appropriate type of filling wall [25]. In addition, using SolidWorks software (https://www.solidworks.com/zh-hans Last accessed date: 10 May 2023), a 3D model of the rock mass can be established, and then the properties of the support pressure region can be analyzed and verified [14].

Through coal seam stress measurement, anchoring force measurements, roof separation monitoring, microseismic monitoring, and other technologies, the distribution law of coal mine support pressure can be detected. Each technology has its own advantages and limitations in terms of accuracy, ease of use, and costs [19,26,27]. The coal seam stress measurement provides direct information regarding the stress state of the coal seam and surrounding strata, and it can be used to understand the overall distribution of the support pressure of the working face. However, stress measurement requires a comprehensive understanding of the geological structure and properties of coal seams, and cannot provide real-time information regarding the distribution and change in support pressure [28,29]. The anchoring force measurement provides real-time information about the distribution of support pressure by measuring the force applied on the support unit of the working face. This technology is relatively easy to implement and can provide valuable information to adjust the support system to respond to changing conditions. However, the quality of the sensor and the calibration of the measuring system may limit the accuracy of the anchoring force measurement [30,31]. Roof separation monitoring is used to measure the displacement and deformation of the roof strata in the working face, and can be used to detect a potential roof collapse. This technology is relatively easy to implement and can provide real-time information about the change in support pressure distribution. However, roof separation monitoring cannot provide complete support pressure distribution. It can only provide information about roof strata, but not the overall stress state of coal seams [32,33].

Microseismic monitoring includes the use of sensors to detect and record small seismic events, such as those caused by rock fracture or the movement of supporting elements of the working face [34]. This technology can provide real-time support pressure distribution information and provide valuable insights for the study of the geological structure and properties of coal seams. However, the accuracy of microseismic monitoring may be limited by the quality and location of sensors, and the interpretation of seismic data may require advanced seismological knowledge [35,36]. Microseismic technology has been ap-

plied in the field of coal mining to monitor and analyze the distribution and evolution of support pressure in working faces [37]. The application of microseismic technology in coal mining has made encouraging achievements in improving our understanding of the distribution and evolution of support pressure, and in predicting and preventing potential damage or collapse [38–40].

Rockburst monitoring is an important part of rockburst control. By using microseismic monitoring, stress monitoring, drilling cuttings monitoring, and other technologies, as well as using a microseismic monitoring system, a stress monitoring system, and other equipment, the distribution and evolution law of the support pressure can be understood [41,42]. At the same time, with the development of computer technology, deep learning technology has also rapidly developed in microseismic event classification, positioning, and rockburst monitoring and early warning [43,44]. It not only provides a scientific basis for taking reasonable support measures and using coal mining technology, but also effectively improves the safety and stability of a fully mechanized mining face.

Based on this, the North China Institute of Science and Technology collaborated with a certain mine to research the prediction and prevention of rockburst hazards in the vicinity of deep fully mechanized mining faces. In order to understand the evolution and distribution pattern of the surrounding rock supporting pressure at the fully mechanized mining face, this study conducted on-site measurements of microseismic monitoring data during the advancement of the 1300 working face using microseismic monitoring technology. At the same time, a theoretical calculation model of dynamic and static supporting pressure in longwall mining was constructed to calculate and analyze the distribution range and evolution pattern of supporting pressure. Using coal stress monitoring, anchor force monitoring, and other means, as well as CT geophysical prospecting and drilling cuttings measurements, the effectiveness of the microseismic analysis results and the accuracy of the aforementioned theoretical model were further verified. Ultimately, a monitoring and early warning system for rockburst hazards at the fully mechanized mining face was proposed based on the distribution and evolution pattern of the supporting pressure. The research results provide an important theoretical basis and practical experience for the prevention and control of rockburst hazards, and safe, efficient mining of the 1300 primary mining face and other similar faces at the mine. They hold significant reference value and have important scientific significance and practical value for accelerating coal resource development and ensuring safe coal mining.

2. Project Profile

2.1. Introduction of the Test Site

In a certain mine in Shandong, the depth of the coal seams that can be mined is generally between −400 to −1500 m. The main coal resources in the mine are mainly concentrated at the −1000 m level or shallower. The average thickness of coal seams in the mine is 10.15 m, and the coal-bearing coefficient is 4.5%. Layer 3 coal is the main and first coal to be mined, with an average thickness of 6.87 m, accounting for 68% of the average total thickness of the coal seams. The thickness of layer 3 coal is 3.96 to 7.88 m, with an average thickness of 6.87 m, and a unidirectional compressive strength of σ_c = 15.82 MPa. The tendency index of rockburst is around WET = 4.58, and the coal seam structure is relatively simple.

According to the exposure of the coal seam during the excavation of the roadway, it can be observed that there is a hard coal seam approximately 0.55 m thick at a distance of around 2.3 m from the floor of the coal seam. The coal seam and roof-to-floor at the working face are as follows: main roof, generally more than 10 m of fine sandstone; immediate roof, generally around 1 to 2 m of sandy mudstone; immediate floor, generally about 1 to 6 m of muddy sandstone or mudstone, fine sandstone, and muddy sandstone interbedded; main floor, generally more than 7 m of powder sandstone. It belongs to the structure of soft immediate roof-to-floor and hard main roof-to-floor.

The initial mining face, designated as the 1300 working face, is the first working face located at the southern wing of the upper part of the primary mining area. The length of

the working face measures 100 m, while the advance distance of mining operations spans 1263 m. The eastern part of the 1300 working face is the 1301 preparatory working face, and its belt transport down chute serves as the drainage alley for the 1300 face. This face mainly mines three coal seams, which greatly fluctuate along the trough due to structural influences. Both horizontal and inclined coal seams are present in the area. The three coal seams are irregular in direction, tending to the northeast and southeast with dips of 6–12°. The 1301 working face starts opening construction from the south at the door mouth of the second contact tunnel on the east side of the 1300 working face drainage alley, with an opening azimuth of 169°. The west side of the tunnel, 80 m from the 1300 working face, is an auxiliary transportation trough with a depth of 860–920 m. The trough is arranged along the coal seam floor and has a coal body with a thickness of 3–5 m.

Numerous domestic and international experts have conducted extensive research on this topic, making progress in understanding the mechanisms behind rockburst occurrences, monitoring, early warning, and prevention methods. However, as technology advances, new challenges and complex problems arise, such as the emergence of increasingly novel coal and rock dynamic disasters, such as the rockburst events in the vicinity of the coal mine's fully mechanized longwall face. As a typical deep mine, this coal mine is seriously affected by rockburst and has suffered several rockburst accidents, as shown in Figure 1. In the period 2014–2015 alone, there were six rockburst accidents, of which the mining of the 1300 working face, induced by the 1301 working face belt transport down chute, caused four rockburst accidents, causing huge economic losses to the mine and seriously threatening the safety production of the mine.

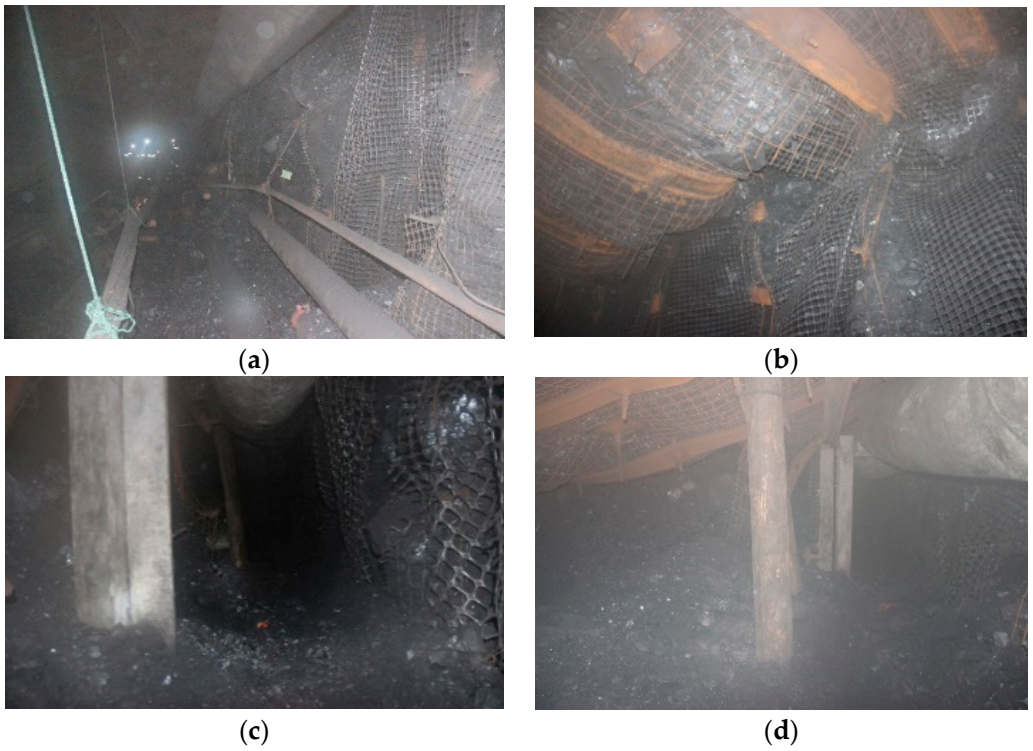

Figure 1. Damage caused by rockburst. (**a**) Equipment damage in the roadway. (**b**) Large deformation of roadway. (**c**) Large deformation of roof fall and floor heave. (**d**) Severe blockage of roadway.

2.2. Rockburst Phenomenon in Adjacent Areas

Since 5 April 2014, various degrees of rockburst events have occurred in the vicinity of the 1300 fully mechanized caving face, which caused varying degrees of damage to the roadway and seriously affected the construction safety of the site.

(1) Event I: Rockburst event of the belt transport down chute on the 1301 working face on 5 September 2014

At 13:36 on 5 September 2014, a rockburst event occurred along the belt chute of the 1301 working face. The site monitoring location of the focal point was located in the coal pillar area 80 m south of the No. 2 contact lane of the drainage alley of the 1300 working face and 30 m east of the 1300 working face, as shown in Figure 2. As a result of the accident, roof subsidence and internal extrusion occurred to different degrees, within the range of 10 m to the north and 120 m to the south of the contact lane 2# of the drainage alley in the 1300 working face. The phenomena of internal extrusion and floor heave occurred in the more serious area (38 m in total), with an internal extrusion volume of 200 mm and a floor heave volume of 150 mm. The local roof and two-sided mesh were damaged by coal body falling. According to the field survey, the roadway with serious damage essentially corresponded to the goaf of the working face.

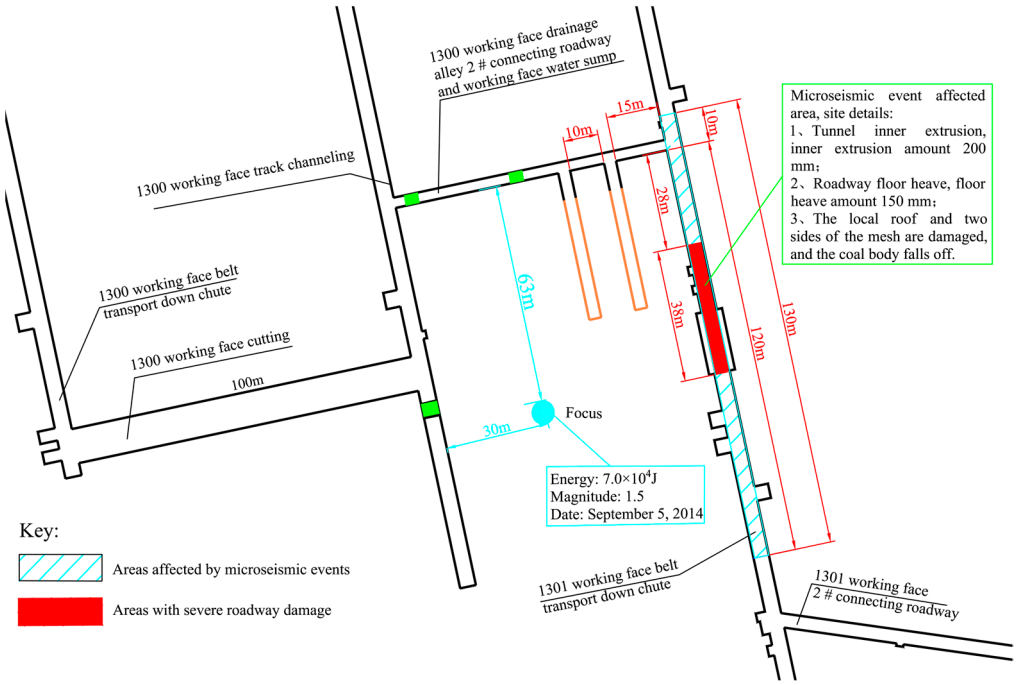

Figure 2. 1301 working face belt transport down chute Case 1.

(2) Event II: Rockburst event of the belt transport down chute on the 1301 working face on 14 September 2014

At 0:40 on 14 September 2014, a rockburst event occurred in the belt channeling of the 1301 working face. On 14 September 2014, the event caused a large area of roof subsidence, a two-sided internal extrusion phenomenon, partial roof and two-sided mesh breakage, and coal body falling within 90–140 m (50 m in total) south of contact lane 2# of the drainage alley of the 1300 working face. The event location is shown in Figure 3.

The incident occurred at the belt transport down chute of the 1301 working face, which was separated by an 80 m mined-out area from the 1300 workface mined-out area. According to traditional theory analysis, the 1301 belt transport down chute should not be easily affected by the lateral support pressure of the 1300 mined-out workface, but in reality, during the process of mining out the 1300 workface, multiple rockburst events and frequent mine pressure appear at the 1301 belt transport down chute, which cannot be explained by traditional theory analysis.

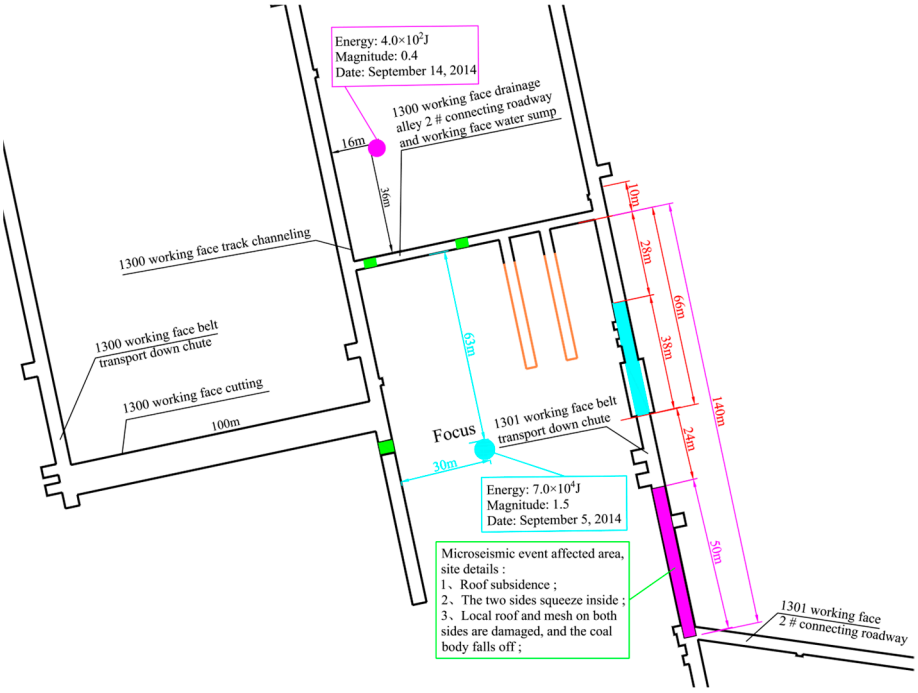

Figure 3. 1301 working face belt transport down chute Case 2.

2.3. Mechanism Analysis

Regarding the mechanism of rockbursts, it is generally recognized that they are a stress problem; that is, when the stress in the coal meets the critical stress condition for rockburst, a rockburst will occur. According to traditional rock pressure theory, rockbursts frequently occur within 60 m in advance of the solid roadway in the mining process of deep well working faces, while rockbursts do not frequently occur in other areas. This concept cannot be applied to rockbursts in the vicinity of fully mechanized caving faces. Therefore, although the essence of the rockburst problem in the vicinity of fully mechanized caving faces is still a stress problem, its "force source" is different from the original calculation of lateral abutment pressure, so the evolution and superposition of stress should be considered. According to the mining influence range shown by the above microseismic monitoring results, the lateral abutment pressure of the goaf at the 1300 working face should be greater than 120 m, which is beyond the protection range of the 80 m coal pillar. Therefore, the belt transport down chute in a 1301 working face is under the influence of the lateral abutment pressure in a 1300 goaf.

It can be seen that the root cause of rockbursts in the area adjacent to the fully mechanized caving face (the belt transport down chute in the 1301 working face) is the superposition of the original rock stress in the area and that the lateral abutment pressure in the 1300 goaf exceeds the critical stress condition for rockburst. In the final analysis, the essence of rockburst is still the stress problem. The above abnormal ore pressure phenomenon still needs to be explained from the perspective of stress evolution or superposition. Since the traditional abutment pressure theory cannot explain these phenomena, this paper tries to discuss the evolution law of abutment pressure in longwall stope, hoping to essentially reveal the distribution characteristics of abutment pressure in longwall stope, so as to provide a scientific basis for the prevention and control of rockbursts in deep wells.

Based on this, the North China Institute of Science and Technology and a mine jointly carried out research on the prediction of and prevention technology for rockburst in the area near the fully mechanized caving face of a deep well. Aimed at the issue of rockburst accidents occurring several times near the 1301 belt passage of the 1300 fully mechanized caving face in a mine, taking the evolution and distribution law of abutment pressure in the surrounding rock of the 1300 fully mechanized caving face in the deep well as the breakthrough point and relying on microseismic monitoring technology, the distribution

characteristics of abutment pressure in the surrounding rock of 1300 working face were measured and the mechanism of rockburst in the adjacent area was revealed. The dynamic and static abutment pressure calculation models of the longwall stope are constructed to analyze the internal relationship between the advancement of the deep well fully mechanized mining face and the impact pressure in adjacent areas, and a corresponding warning system and prevention measures are proposed.

3. Analysis of Abutment Pressure Evolution Law Based on Microseismic Monitoring

The migration and evolution process of the stress field is intrinsically related to the evolution of the vibration field and the fracture field. The evolution law of abutment pressure in a longwall stope can be revealed by the spatial distribution of the fracture field, and the spatial evolution of the fracture field can be reflected by the results of microseismic monitoring. Therefore, statistical analysis is conducted on the microseismic monitoring data of the 1300 stope working face in the process of advancing, so as to obtain the mining influence range of the fully mechanized caving working face and the microseismic response rule when the working face passes through the fault, which provides a basis for the evolution and distribution characteristics of stope abutment pressure.

3.1. Analysis of the Mining Influence Range in the Working Face

Taking the microseismic monitoring data from 21 May 2015 to 20 June 2015 as an example, during this period, the working face advanced a total of 87.2 m. Figure 4 shows the plane projection of microseismic events in this time period. The scatter points with different colors reflect the analysis results of a single microseismic event. The corresponding is the energy magnitude of a single microseismic event, which is taken as lg(E). E represents the magnitude of the seismic event energy, measured in Joules. The advance rupture envelope and lag rupture envelope of the coal and rock mass are shown in the envelope area of the red and green dashed lines, among which the advance severe impact area is delineated by the red solid line, indicating a higher frequency of microseismic events, and the lag severe impact area is located in the green solid line area behind the working face.

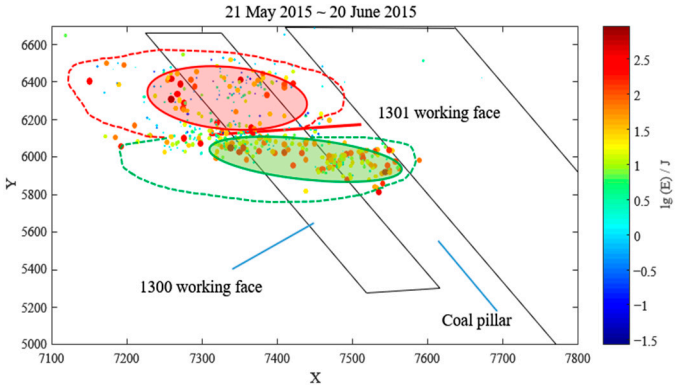

Figure 4. Analysis of the mining influence range of the fully mechanized caving face (microseismic plane projection).

As can be seen from Figure 4, microseismic events are widely distributed, indicating a large mining influence range in the working face, including 430 m in front and 320 m behind the face. There are also a large number of microseismic events outside the auxiliary transportation roadway behind the working face and inside the 80 m coal pillar. This area contains two large faults, Yf1 and Yf2. It is speculated that after the working face passes through the fault, the influence of mining lag induces fault activation again.

Figure 5 shows the profile projection of microseismic events during the mining process of the working face, including the projection along the strike and the dip direction. The red solid line represents the position of the working face, the black solid line represents the unmined coal seam, and the gray solid line represents the completed mining of the coal seam.

The evolution of the spatial morphology of the roof and floor of the solid working face in the mining process can be seen in the figure. As can be seen from Figure 5a, the roof rupture height is about 38 m on average and the floor is about 20 m, and microseismic events are concentrated in the coal pillar area of 80 m. In the 1301 working face, there are concentrated events at the belt transport down chute, indicating that there is a high stress difference near this area. The microseismic activity of the 1300 auxiliary track trough is more intense than that of the belt track trough, which is closely related to the spatial layout of the track trough and the nearby fault activity. Figure 5b further confirms that the mining influence range is about 320 m behind the working face and 430 m in front of it.

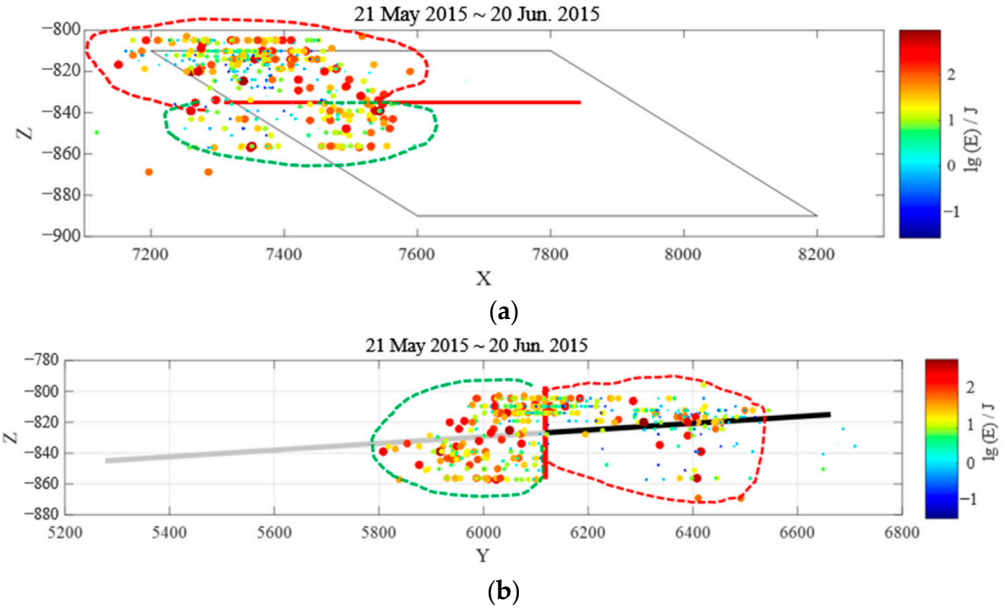

Figure 5. Analysis of mining influence on the fully mechanized caving face (profile projection). (**a**) Projection along the dip profile. (**b**) Profile projection along the strike.

3.2. Analysis of the Microseismic Activity in the Tectonic Region

In order to study the activity signs in the tectonic area during the mining process of the 1300 working face, the microseismic activity in the fault areas of FY15, Yf2, and Yf1 was statistically analyzed. As shown in Figure 6, the FY15 fault obliques through working faces 1300 and 1301. During the mining process, the 1300 working face successively passed FY15 and Yf1, and was affected by the Yf2 fault. In the early stage of mining, the stope was ahead of the principle of abutment pressure in the fault area, but it still induced the occurrence of a large number of small energy vibration events in the fault area, such as the plane projection of microseismic events from January 2014 to October 2014. With the advancement of the working face (1 January 2014–1 December 2014), the FY15 fault was within the influence range of advanced abatement pressure. Mining induced a few large energy events and a large number of small energy events. The spatial distribution of events was consistent with the fault morphology, indicating that mining induced fault activation. When approaching the FY15 fault (December 2014–31 December 2014), a large number of microseismic events were distributed in the rock mass around the working face, with large energy and small energy microseismic events alternately occurring with irregular frequency. Meanwhile, the advanced abutment pressure induced the Yf2 and Yf1 faults 300 m in front. It is speculated that this phenomenon is influenced by two factors: one is the gradual activation and induction of the major FY15 fault, and the other is the high mining rate of 6.4 m/s.

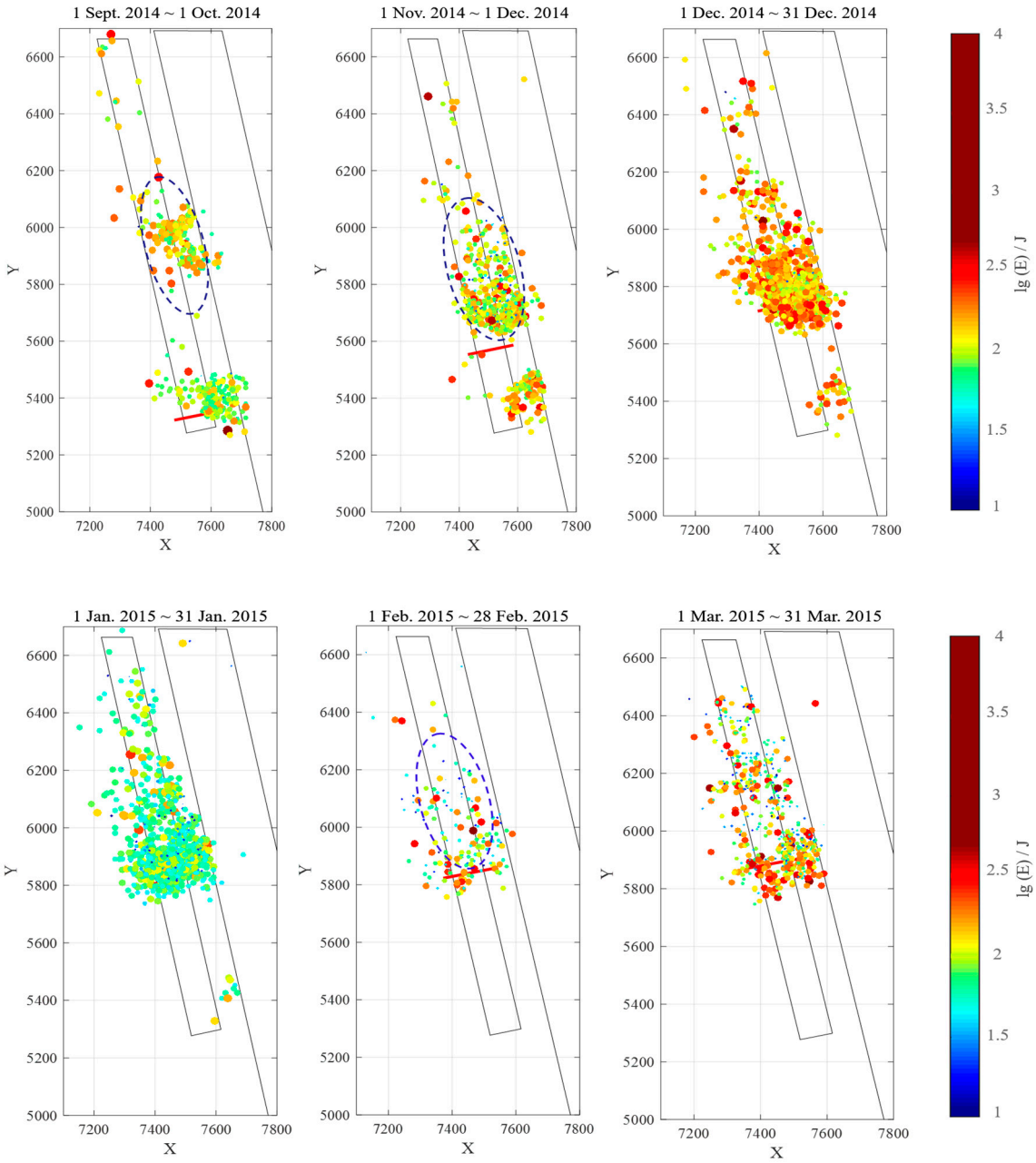

Figure 6. Microseismic distribution diagram of the 1300 working face and the adjacent 1301 working face.

Due to the violent activity of the fault, the 1300 working face implemented the corresponding safety measures in the mining process, reduced the mining speed of the working face to 4.8 m/s, and stopped production for consolidation in the later stage. At this time, although there were still a large number of microseismic events in the working face, the event energy was small, indicating that the high-stress area around the fault was transferred or weakened under the action of artificial "weak thrust" measures. The high-stress concentration was no longer obvious, and the sudden release of the weakened residual potential energy of coal rock mass was not enough to induce large energy events, which also indicates that the rockburst prevention measures effectively inhibited the occurrence of rockburst, such as during the period 1 January 2015–31 January 2015. After passing through the fault, on the one hand, the working face slowed down the speed of thrust mining, waiting for the full evolution of the overlying strata. Meanwhile, the fault was still in the range of the stope pressure relief zone. Therefore, the microseismic events significantly decreased, and some large energy events were suspected to be a rebalancing of the fault

region, such as during the period January 2015–28 February 2015. During the period from January 2015 to 28 February 2015, microseismic activity became active again. On the one hand, the Yf2 and Yf1 faults entered the influence range of advanced abutment pressure; on the other hand, the FY15 fault was under the influence of hysteresis and the severe area.

3.3. Analysis of the Abutment Pressure Distribution Range

The microseismic monitoring system arranged in the field recorded the vibration response of the working face during the mining process. In order to analyze the causes of these accidents, microseismic events were counted on a daily basis and projected onto the planar graph. The results are shown in Figure 7.

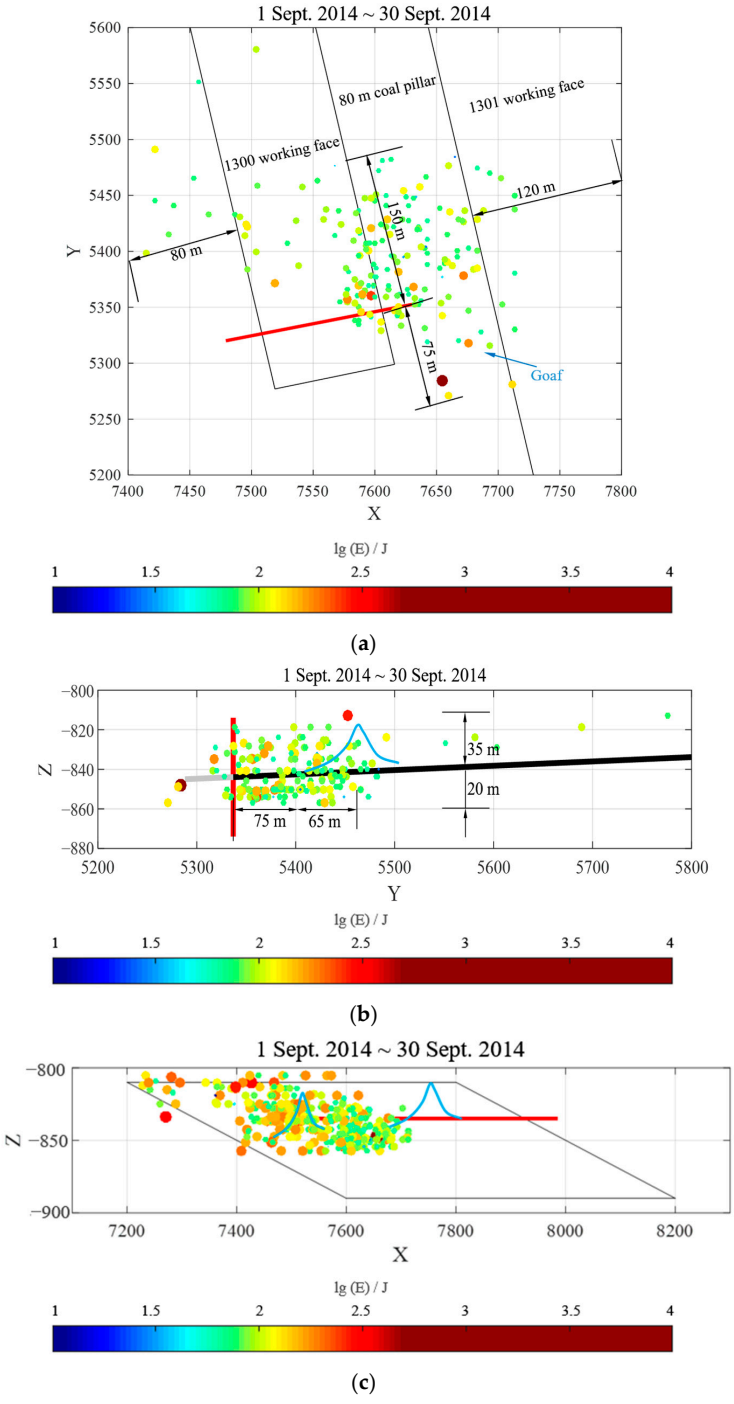

Figure 7. Display of support pressure distribution patterns based on microseismic data analysis. (**a**) Plane projection. (**b**) Strike profile projection. (**c**) Dip profile projection.

(1) Strike abutment pressure distribution

As can be seen in Figure 7, the spatial distribution of microseismic events in the working face stoping process has typical zoning characteristics, and is closely related to the transfer of the mining stress field. The mining influence range is 150 m in front of the working face, 75 m behind the working face, 120 m outside the auxiliary track channeling, and 80 m outside the belt channeling. According to the principle of microseismic event zoning (the correlation between the distribution density of microseismic events and the "blind area"), it can be inferred from Figure 7b that the peak position of strike abutment pressure on the working face is 65 m in front.

(2) Inclined abutment pressure distribution

Combined with Figure 7a,c, the lateral abutment pressure distribution characteristics of the working face can be predicted. As shown in the figure, the mining influence range on both sides of solid coal in front of the working face is wider, and the outer side of the auxiliary track channeling (120 m) is wider than that of the belt channeling (80 m). On both sides of the goaf behind the working face, the microseismic response is not obvious in the belt channeling area, but it is more obvious on the track channeling side, especially in the 80 m coal pillar and 1301 belt channeling, where a large number of microseismic events are distributed. According to the corresponding relationship between the fracture position of the upper strata and the stress of coal, it can be inferred that the peak position of lateral abutment pressure in the goaf is about 65 m away from the goaf.

4. Construction of the Dynamic and Static Abutment Pressure Calculation Model

The accurate acquisition of static and static abutment pressure distribution data is the key to carrying out rockburst risk analysis. The stope roof breaks and turns ahead of time, which causes the coal body to deform and yield, causing the coal body to lose its bearing capacity, and causing the stress to transfer to the deep-forming dynamic abutment pressure. With the increase in the mined-out area, the load on the key layer above the fault zone increases, and the load on the key layer supported by the lower rock layer transfers to both sides and in front, forming static abutment pressure. According to the above analysis, the main reason for rockburst in the adjacent area of the fully mechanized caving face is the superposition of static and static abutment pressures. Therefore, the distribution range of abutment pressure will be calculated and its evolution law will be analyzed by means of theoretical derivation and field measurements.

4.1. Static Abutment Pressure Calculation Model

Before and after the goaf is formed, the load of the roof strata to be borne by the coal seam is constant. As shown in Figure 8, before the goaf is formed, the load of the roof strata is evenly distributed on the coal seam; after the goaf is formed, the load of the roof strata will be transferred to the coal body outside the goaf and the gangue in the goaf.

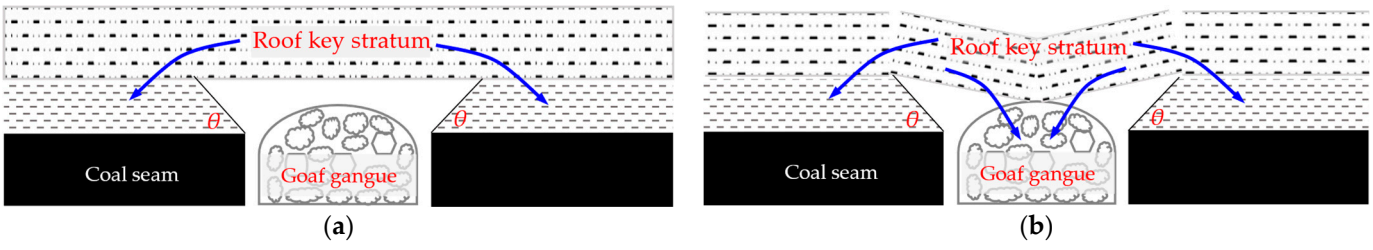

Figure 8. Diagram of critical stratum load transfer [44]. (**a**) Before breaking. (**b**) After breaking.

Abutment pressure σ of the coal body on one side of the goaf is composed of dead weight stress σ_q and stress increment $\Delta\sigma$, which can be expressed as:

$$\sigma = \Delta\sigma + \sigma_q, \quad (1)$$

In the formula, $\Delta\sigma$ is the common sum (MPa) of the stress increment formed by the load of the overhanging part of each key stratum of the stope or the load of the broken block segment transferred to the coal body on one side, namely, $\Delta\sigma = \sum\Delta\sigma_i$; $\Delta\sigma_i$ is the stress increment (MPa) caused by the load transferred to the coal body on one side by the overhanging part or the broken block section of the i th key stratum, i = 1~m.

(1) Gravity stress

The critical stratum in roof strata is the medium of load transfer in roof strata. The static abutment pressure calculation model can be established according to the critical stratum theory and the load transfer characteristics of roof strata, as shown in Figure 9. Before the critical stratum breaks, half of the load in the overhanging part is transferred to the coal body on one side of the goaf.

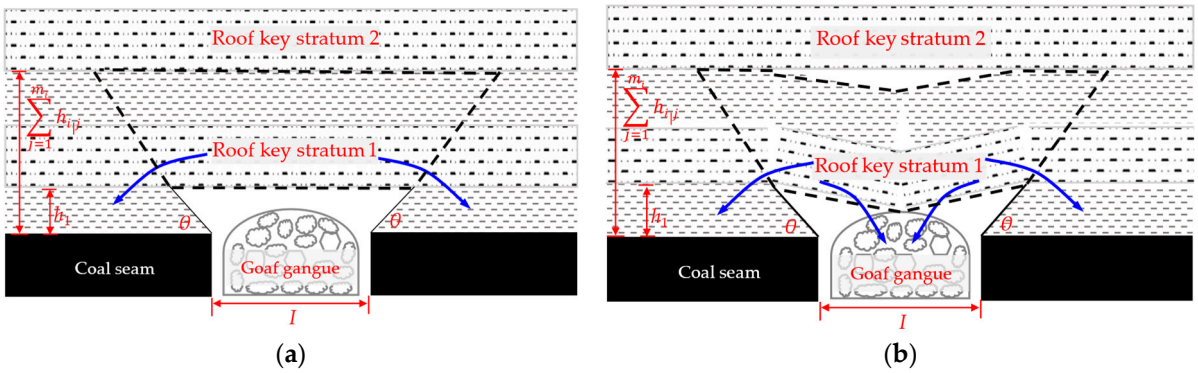

(**a**) (**b**)

Figure 9. Static abutment pressure calculation model [45]. (**a**) Calculation model of the load on the overhanging part of the critical layer before breaking. (**b**) Load calculation model of the critical layer fault block segment.

Let the load of the hanging part of key stratum i be q_i, then the load transferred to the coal body on one side of the goaf is $Q_i = q_i/2$. q_i is calculated as shown in Equation (2).

Suppose that the distance from the ith key stratum to the coal seam is H_i, and the rock formation controlled by it has m_i rock layers, denoted as $c_{i|j}(j = 1, 2, \ldots, m_i)$ from bottom to top, then

$$q_i = \gamma\left[2\left(H_i + \frac{1}{2}\sum_{j=1}^{m_i} h_{i|j}\right)\cot\theta + I\right]\sum_{j=1}^{m_i} h_{i|j}, \tag{2}$$

where, $h_{i|j}$ is the thickness of rock layer (m), I is the width of working face (m), θ is the fracture angle, and γ is the bulk density.

After the key stratum is broken, half of the load of the broken block section is transferred to the coal body on one side of the goaf. Assuming that the length of the fault block section of the i th key stratum is L_i and the load is q_i', then the load $Q_i = q_i'/2$ transferred to the coal body on one side of the goaf is transferred. q_i' is calculated as follows:

$$q_i' = \gamma\left(L_i + \frac{1}{2}\cot\theta\sum_{j=1}^{m_i} h_{i|j}\right)\sum_{j=1}^{m_i} h_{i|j}, \tag{3}$$

(2) Stress increment

When there are multiple key layers in the stope roof strata, the stress increment generated by each key layer is superimposed, as shown in Equation (4), and $\Delta\sigma$ is obtained. The formula for calculating σ_q is:

$$\sigma_q = \begin{cases} \gamma I & (x = 0 \to I\cot\theta) \\ \gamma x\tan\theta & (x = I\cot\theta H\cot\theta), \\ \gamma H & (x = H\cot\theta\infty) \end{cases} \tag{4}$$

It can be seen that the calculation formula of static abutment pressure is a group of piecework functions. The distribution characteristics of static abutment pressure are related to the fracture angle, the number of key layers, the position of key layers, the thickness of each rock group, the length of the broken block, and the buried depth.

4.2. Dynamic Abutment Pressure Calculation Model

Under the action of abutment pressure, the coal body on both sides or in front of the goaf tends to move to the stope and forms the stress limit equilibrium zone. According to the characteristics of coal wall stress transfer to the deep coal body after yield, a dynamic abutment pressure calculation model is established by using the limit equilibrium method, as shown in Figure 10, where p_0 is the coal wall support resistance (MPa), x is the distance (m) between the investigation point and the coal wall, x_t is the distance (m) between the influence of abutment pressure, and x_0 is the distance (m) between the peak position and the coal wall. N_0 is the vertical supporting force of the coal wall (MPa), γ is the average bulk density of the overlying rock (MN•m^3), H is the buried depth of the stope (m), k is the stress concentration factor, and σ_y is the vertical stress in the coal body (MPa). The influence range of dynamic abutment pressure can be divided into three parts: the 0~x_0 part is the plastic region, and the abutment pressure presents exponential function distribution. The part x_0~x_t is the elastic active region, and the abutment pressure is negative exponential function distribution. The part x_t~∞ is the stress region of the original rock, and the abutment pressure presents constant function distribution.

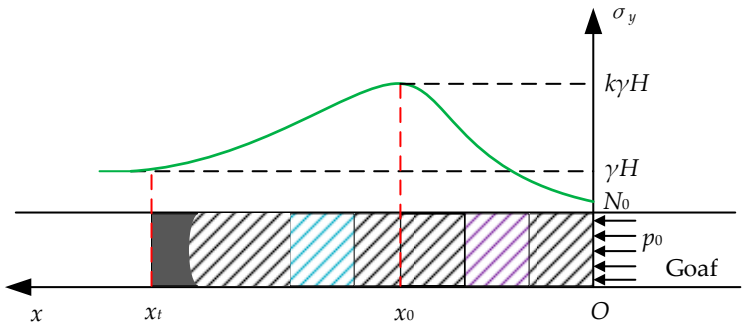

Figure 10. Dynamic abutment pressure calculation model [45].

Based on the above analysis and considering the boundary conditions, the calculation model of abutment pressure distribution can be obtained as follows:

$$\sigma_y = N_0 e^{\frac{2fx}{M}\left(\frac{1+\sin\varphi}{1-\sin\varphi}\right)}, \tag{5}$$

where, σ_y is the vertical stress of the coal body (MPa), M is the thickness of the coal seam (m), f is the friction factor of the layer.

Assume that 0 is the lateral pressure coefficient, $\sigma_x = \lambda\sigma_y$ in the elastic region, then

$$\sigma_y = k\gamma H e^{-\left[\frac{2f\lambda}{M}(x-x_0)\right]}, \tag{6}$$

The influence distance of abutment pressure is as follows:

$$x_t = x_0 + \frac{M}{2f\lambda}\ln k, \tag{7}$$

4.3. Case Checking

For a heavy topsoil stope, the rock strata above the rupture range of the roof can be simplified into one rock group. Considering the large thickness of the bedrock, the displacement angle α is around 82°. The mining depth is 860 m and the inclined length of the working face is 100 m. Other calculation conditions are as follows: coal seam thickness

M = 7.0 m, working face depth H = 860 m, working face width I = 100 m, overburden average bulk density γ = 0.025 MN/m^3, fracture angle θ = 82°, layer friction coefficient f = 0.2, internal friction angle φ = 28.5°, and side pressure coefficient γ = 0.5. The stress concentration coefficient k = 2. The vertical supporting force of coal wall N_0 is calculated by the static abutment pressure calculation formula. The calculating interval of the independent variable in the final calculated segment function is:

$$[0\ 7],\ [7\ 63],\ [63\ 126],\ [126\ 130],\ [130\ \infty], \tag{8}$$

The calculation process is simplified, and the rock above the fracture range is taken as a rock group, so its thickness M1 is around 800 m. By plugging working face parameters into Equations (5)–(7), and taking rock bulk density γ as 2.5 t/m^3, the specific lateral abutment pressure calculation formula can be obtained as follows:

$$\sigma = \begin{cases} 1.25 + 0.57x & (0,\ 7) \\ 0.75x & (7,\ 63) \\ 71.6 - 0.39x & (63,\ 126), \\ 0.18x & (126,\ 130) \\ 21.5 & (130,\ \infty) \end{cases} \tag{9}$$

Through calculation, the lateral abutment pressure distribution of the coal body on one side of the 1300 goaf is obtained, as shown in Figure 11. It can be seen from the figure that the peak position of lateral abutment pressure of the coal body outside the goaf is about 63 m away from the goaf, and the peak value of abutment pressure is about 47 MPa. The low stress area is 0–28 m away from the goaf. The abutment pressure affected area is 28 m–130 m away from the goaf. The original rock stress area is 130 m away from the goaf. This monitoring result is consistent with the mining influence range revealed by the microseismic monitoring results.

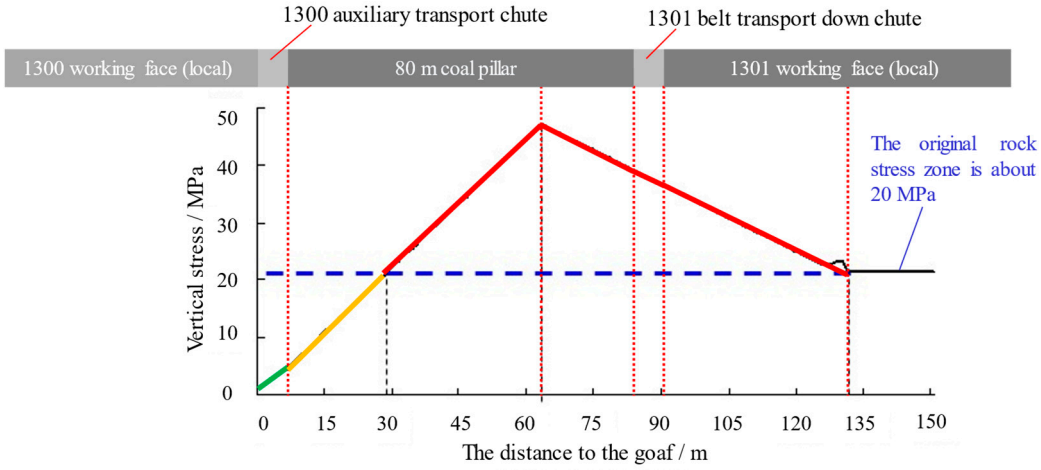

Figure 11. Lateral abutment pressure curve of the 1300 goaf.

The distance between the outer section of the belt transport down chute in the 1301 working face and the 1300 goaf is 80 m, which is just within the influence range of abutment pressure on the side of the 1300 goaf. The vertical stress here is about 40 MPa, much higher than the uniaxial compressive strength of the coal seam, 15 MPa. Therefore, rockburst can easily occur during the driving of the outer section of the belt transport down chute in the 1301 working face.

Based on the above calculation results, the influence areas of the goaf in the 1300 working face are divided, and the final goaf influence danger zone is shown in Figure 12. It can be seen that the duct of the 1301 belt transport down chute is completely under the influence range of the goaf of the 1300 working face, which further confirms the root cause of the previous multiple rockburst events.

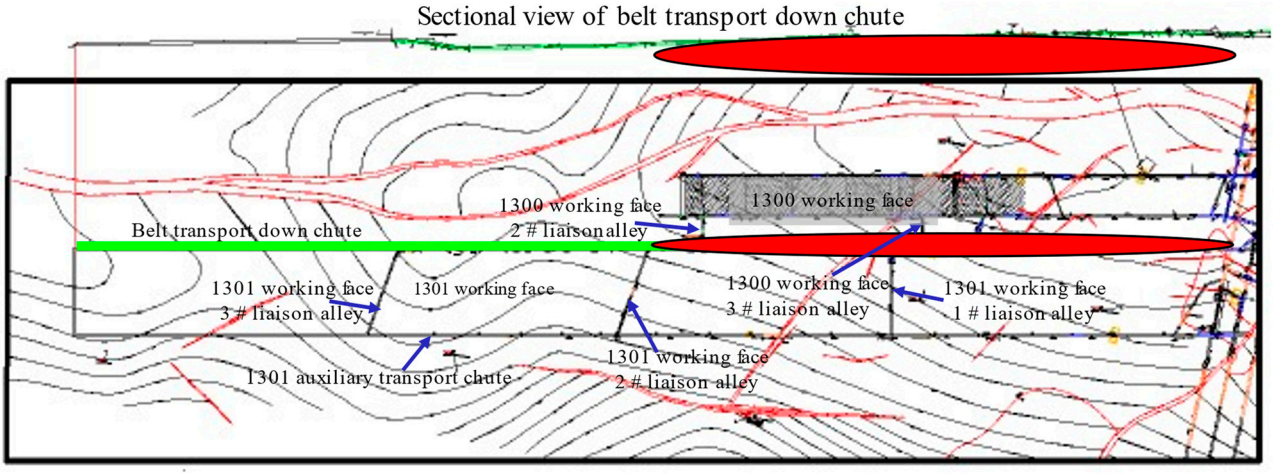

Figure 12. Goaf affected area.

5. Other Monitoring Analysis and Measurement Verification

5.1. Analysis and Comparison of Other Monitoring Means

In order to further verify the accuracy of the above theoretical model and microseismic monitoring results, a comparative analysis was carried out with the results of other on-site monitoring methods, including online stress monitoring, bolt force monitoring, CT detection, etc. At the same time, the stress state of the coal body was measured and tested by the amount of drilling cuttings.

(1) Analysis of the results of online stress monitoring methods

According to the analysis of the field observation results, the initial weighting of the 1300 working face on 15 September, the sliding head advance distance (from the original cutting hole) was 36 m, the sliding tail was 41.6 m, and the pressure step was 38.8 m (from the original cutting hole). Through the analysis of the observation results of five consecutive periodic weightings, it is inferred that the pressure step of the 1300 working face is as shown in Table 1.

Table 1. 1300 working face periodic weighting statistics.

Periodic Weighting	First	Second	Third	Fourth	Fifth
Periodic pressure step (m)	21.6	23.6	17.6	19.9	14.1
Average value (m)			19.4		

In order to monitor the stress change in the coal body of the 1300 working face in real time, the KJ550 online stress monitoring system was used to monitor the working face in real time. As shown in Figure 13, the borehole stress meters of the system were placed in the coal seam to be mined in the upper and lower level driveways, with a measurement station spacing of 25 m. As the working face advances, real-time monitoring and early warning of impact pressure were conducted in the advance influence zone of the working face. Measurement point arrangement: a No. 1 measurement station was set up 30 m away from the working face cutting end, and one measurement station was arranged every 25 m outward (with an allowable error of ±3 m). Each measurement station had two measurement points, with borehole stress meters installed at depths of 7 m and 13 m, respectively, and spaced 2 m apart. As the working face advanced, the system was promptly dismantled and moved forward, ensuring a monitoring range of no less than 200 m.

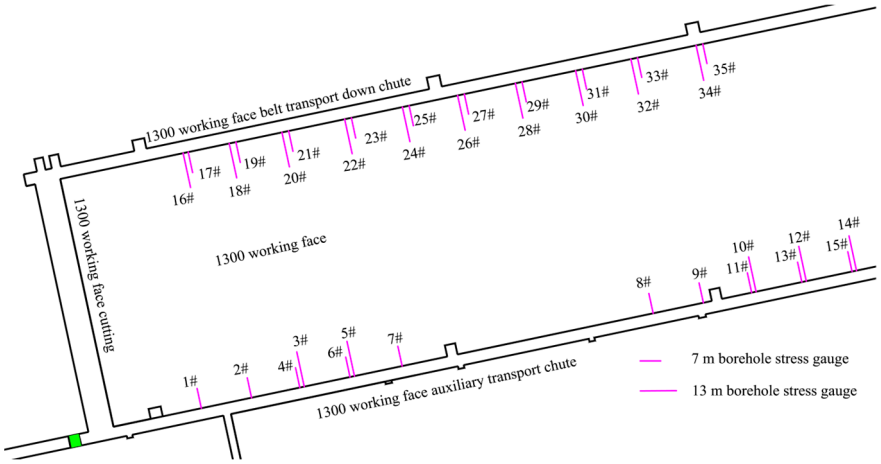

Figure 13. The location distribution of measuring points in the real-time monitoring of and warning system for rockburst.

The stress sensor monitoring data showed that the stress began to rise at a distance of about 60 m from the cutting end, reached its peak at about 20 m from the cutting end, and then declined. This preliminary analysis indicated that the impact zone of the 1300 working face was 60 m, and the stress peak appeared at a distance of about 20 m from the working face. However, in complex geological areas, the influence range was larger due to mining-induced stress, reaching approximately 90 m.

(2) Analysis of observation results of rockbolt dynamometer

In addition, according to the observation of the rockbolt dynamometer, during most of the observation period, the rockbolt dynamometer hovered around the initial rockbolt force, and the working resistance of the rockbolt near the coal wall of the working face rapidly rose, with typical rising inflection points. At a certain distance from the coal wall of the working face, the working resistance of the rockbolt rod slightly fluctuated. The classification and statistical results of the rockbolt rod working resistance are shown in Table 2 below.

Table 2. 1300 working face periodic weighting statistics.

Measure Point	Tail Entry			Belt Transport Down Chute			
anchor bolts dynamometer	4#	6#	Average value	7#	8#	10#	Average value
Distance from coal wall when affected by mining/m	60.3	41.6	50.95	40.4	42.5	64.5	49.13
Distance from stress peak to coal wall/m	32.3	26.1	29.2	26	24.9	19.7	23.53

It can be seen from the statistical results in Table 2 that the position of the working resistance of the tail entry anchor bolts is about 50 m away from the coal wall of the working face under the influence of mining, and the peak stress is about 29 m. Meanwhile, the working resistance of anchor bolts in the belt transport down chute is affected by mining-induced stress at a distance of approximately 49 m from the coal wall of the working face, with the stress peak occurring around 23 m.

(3) Comprehensive comparative analysis results

The field measurement results of the mining influence range and the distribution characteristics of the abutment pressure of the solid working face are summarized and listed in Table 3. It can be seen from the table that the mining influence range obtained from microseismic monitoring is basically consistent with the corresponding results obtained from

dynamic stress monitoring. The distance from the peak position of abutment pressure to the coal wall and the influence range of abutment pressure obtained by microseismic monitoring are larger than those obtained by dynamic stress monitoring. Therefore, it can be inferred that there are two bearing pressures in the surrounding rock of the working face, namely, dynamic bearing pressure and static bearing pressure.

Table 3. Comparison of field measurement results.

Monitoring Means	Mining Influence Range/m		Peak Position of Supporting Pressure/m		Influence Reange of Supporting Pressure/m	
	Pull Ahead	Side Direction	Pull Ahead	Side Direction	Pull Ahead	Side Direction
Dynamic stress monitoring	>90	–	20	–	>20	–
Dynamometer, etc.	>50	–	26.5	–	>26.5	–
Microseismic monitoring	130	120	65	65	>65	>65

"–" in the table is the part not measured.

In fact, the commonly mentioned abutment pressure is dynamic abutment pressure, which is formed in a short time with the advancement of the working face. For general working faces, the distance from the strike peak position to the coal wall is about two to three times the mining height, and the distance from the lateral peak position to the goaf is 15 to 20 m. In addition to the dynamic abutment pressure, there is also a static abutment pressure in the surrounding rock of the working face, which is formed by the weight transfer of the high roof. The distance from its peak position to the coal wall is about two to four times the distance from the peak position of the dynamic abutment pressure to the coal wall.

5.2. Analysis of Rockburst Hazard Sources Based on CT Technology

In order to further test the distribution characteristics of lateral abutment pressure in the goaf of the 1300 working face, the distribution characteristics and hazard degree of rockburst hazard sources in the 1301 working face were measured by seismic CT technology. Figure 14 shows the distribution of rockburst risk index C in the detection area of the 80 m wide coal pillar and the 1301 working face. The magnitude of the hazard index detected by seismic CT is closely related to the degree of stress concentration. Therefore, the magnitude of stress concentration in this area can be inferred from the hazard index of rockburst. The danger index of rockburst in the detection area is represented by blue to red, from small to large (that is, stress distribution from small to large). The maximum value of C in the area is 0.7 and the minimum value is −0.5.

The rockburst hazard index of most areas in the survey area is less than 0.75, but the rockburst hazard index of coal and rock strata in nearly one-fifth of the survey area is $0.5 \leq C < 0.75$, and the above areas are in the middle of the rockburst hazard level. Projecting more than three times the events since 2015 into the C distribution map, it can be seen that the microseismic events are mostly concentrated in the 80 m large coal pillar, the connecting roadway in the 1301 working face, and near the fault structure, especially in the 1301 belt transport down chute. This is because the corresponding area of the coal pillar in the 1301 working face and the 80 m section is comprehensively affected by the lateral bearing pressure, the structure, and other factors of the 1300 working face, the stress distribution is complex, and the risk of rockburst is higher than in other areas, which is consistent with the borehole stress detection results.

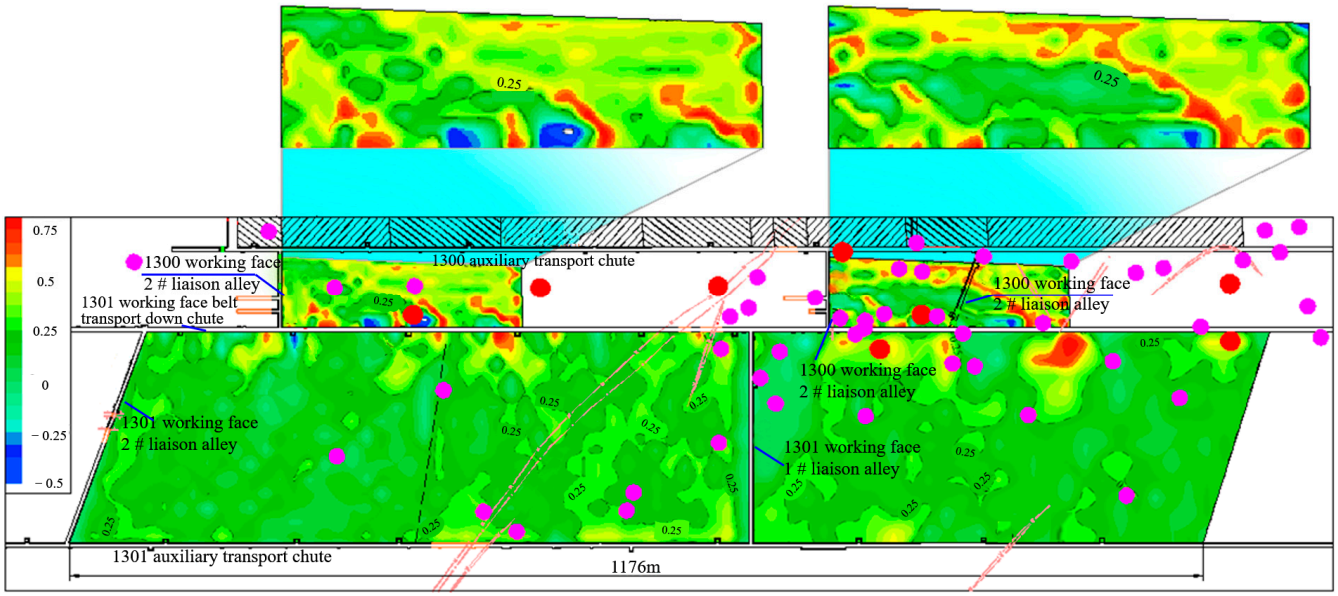

Figure 14. Index distribution map of rockburst risk in the 1301 working face detection area based on seismic CT technology.

In order to verify the conclusion of the seismic CT technology evaluation on the rockburst risk of coal and rock strata, the borehole stress detection test results and seismic CT detection results were compared and analyzed, as shown in Figure 15. According to the number of drilling cuttings and whether there is a dynamic phenomenon in the process of drilling cuttings, the range of the stress concentration area in the surrounding rock of the roadway is defined. It can be seen from Figure 14 that within the range detected by the drilling cuttings method, the area where the drilling cuttings exceed the limit or where dynamic phenomena occur is generally consistent with the distribution of the rockburst hazard area detected by the seismic CT technology, which verifies the reliability of the evaluation method.

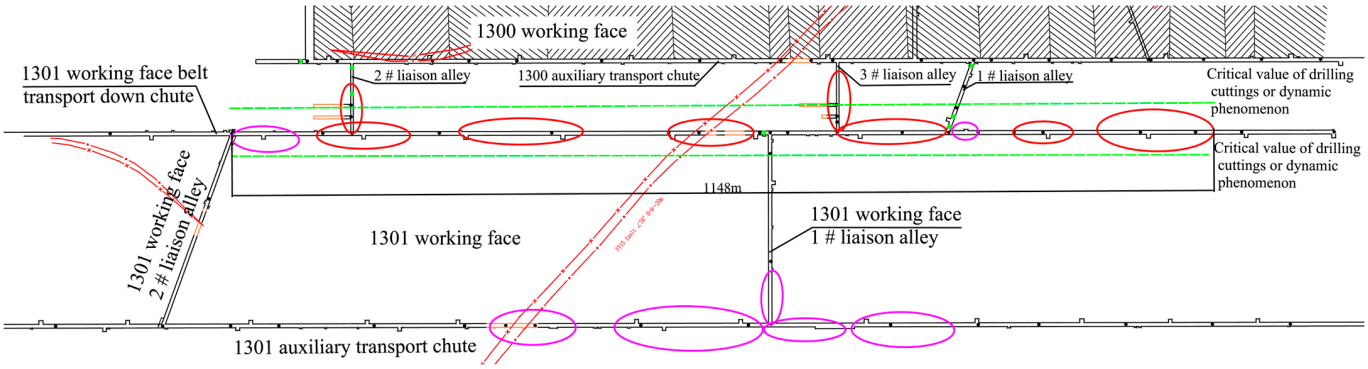

Figure 15. Drilling cuttings test of the wide coal pillar and impact hazard layout of the 1301 working face detection area.

The adjacent area affected by the lateral abutment pressure of the 1300 goaf was detected using the above two methods. The two methods corroborated the previous analysis results; that is, the distribution range of the lateral abutment pressure of the 1300 working face exceeded the 80 m coal pillar protection area, and the belt transport down chute of the 1301 working face was under the influence range of the lateral abutment pressure, which is the root cause of frequent rockburst events in this area.

5.3. Field Measurement and Inspection of Coal Drilling Cuttings

In order to test the correctness of the calculation model of lateral abutment pressure in the longwall stope, an experimental study on coal body stress detection was carried out in the belt transport down chute of the 1301 working face in July 2016; that is, drilling was carried out in the coal pillar area 80 m on both sides and in the 1301 working face near the belt transport down chute; the stress state of this area was tested.

The site drilling construction parameters were as follows: the drilling hole was 1.2–1.5 m above the floor, constructed along the dip angle of the coal seam and perpendicular to the side (the east side is 4–6° lower, the west side is 4–6° upward), the hole depth was 60 m, and the hole diameter was Φ 80 mm. Drilling construction was carried out from south to north in sequence, with a spacing of about 50 m. A total of 17 boreholes were drilled. Except for #7 and #10 boreholes drilled in the 1301 working face, the remaining boreholes #1–#6, #8, #9, and #11–#17 were drilled in the 80-m coal pillar area, as shown in Figure 16. For the convenience of description, the boreholes are divided into two groups, of which boreholes #1–#6, #8, #9, and #11–#17 in the 80-m coal pillar area are Group A, and the boreholes #7 and #10 in the 1301 working face are Group B.

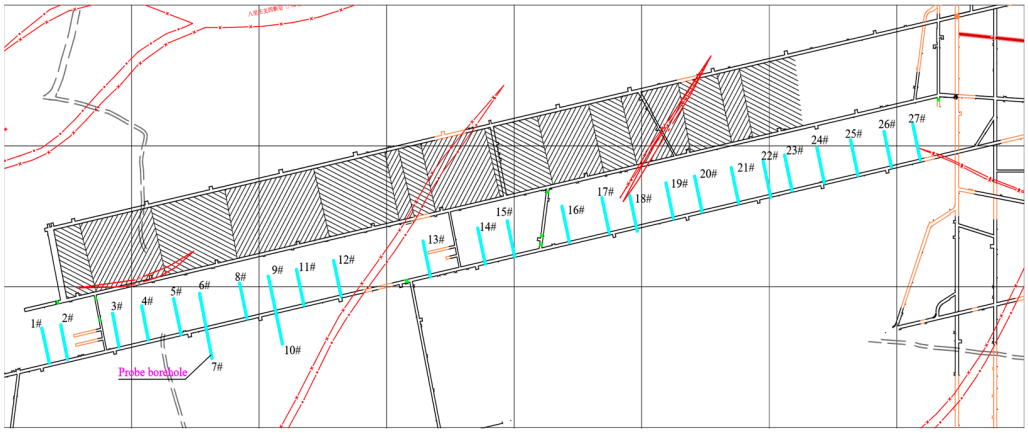

Figure 16. Construction scheme of coal body stress detection in the 80-m coal pillar area.

According to the principle of the drilling cuttings method, there is a quantitative relationship between the quantity and particle size of pulverized coal discharged from the borehole, the relevant dynamic effects (such as the coal gun, the suction drill, and the sticking drill), and the stress state of the coal body. On this basis, in the test process, the coal particle size, the number of coal guns, the strength of coal guns, and the dynamic phenomenon during the drilling process are respectively counted with a unit depth of 5 m to judge and describe the current drilling depth. After the test, the data collected on the site were sorted and analyzed, and the relevant results are shown in Figure 16. The white, yellow and red areas in the figure represent the stress concentration status in the coal body, in which the white area shows no stress concentration, and the red area is the highly concentrated area.

From an analysis of Figure 17, it can be seen that the boreholes of Group A in the coal pillar area are essentially in the original rock stress state within the range of 1–20 m, and there is no obvious stress concentration, which is related to the recent boreholes in this area. The 1301 belt in this area was drilled to a depth of 20 m along the inner and outer sides of the belt transport down chute for pressure relief, resulting in the transfer of stress load within 20 m, so a relative 20-m wide "low-pressure zone" appeared in the chart. The stress state in the coal body changes after the hole depth of 20 m. Take 1# drill hole as an example to illustrate that, with the increase in hole depth, the particle size of coal powder changes from powder to small particles, and large particles appear when the hole depth reaches 46 m. The number and strength of coal guns also gradually increase, accompanied by the strong phenomenon of suction drilling. It can be determined that there is still stress

concentration in the 80-m coal pillar outside the 1301 belt slot. That is, the range of the lateral abutment pressure in the 1300 goaf is more than 80 m, which exceeds the width of the 80-m protective coal pillar and directly affects the adjacent 1301 working face.

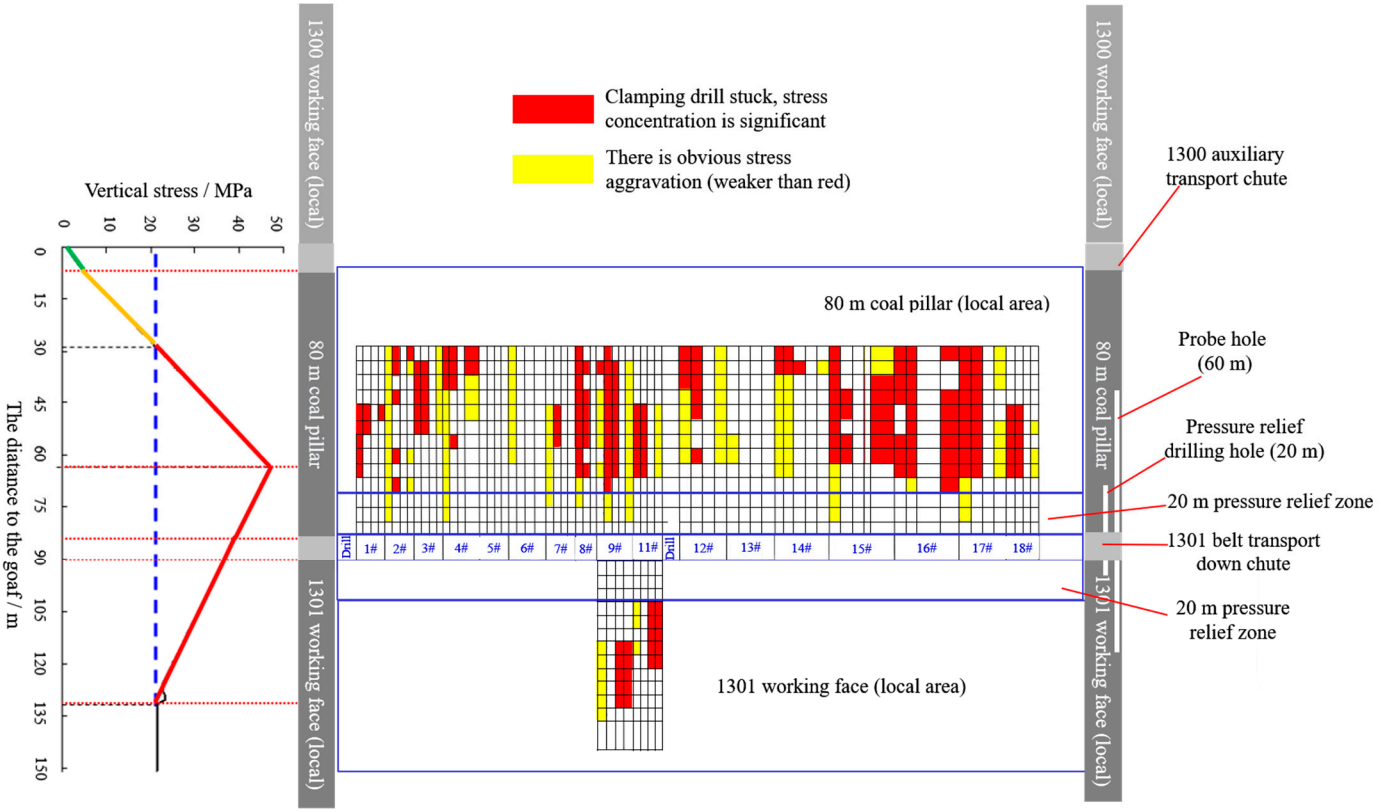

Figure 17. Comparative analysis of drilling cuttings in coal.

At the same time, the data of the Group B boreholes (7#–10# boreholes) were analyzed. Group B is located in the coal body of the 1301 working face. The analysis results show that the coal body within 60 m of the 1301 working face is still within the influence range of the lateral abutment pressure of the 1300 goaf. In addition to the 80-m coal pillar and the roadway width, the measured lateral abutment pressure of the 1300 goaf is around $80 + 60 + 2 \times 4.8 = 150$ m. This is consistent with the 130-m results obtained by theoretical calculation, which also proves the correctness of the calculation model of lateral abutment pressure in the fully mechanized caving face.

6. Engineering Application and Case Analysis

6.1. Construction of the Rockburst Early Warning System

By analyzing the microseismic data of the 1300 working face during mining, the law of microseismic energy release in the stope is analyzed, the critical values of the microseismic daily release energy and energy per unit propulsion degree are determined, and the ARAMIS M/E microseismic monitoring and early warning index system during the mining of the coal mine's solid working face is established. Finally, 95.4% and 99.7% of the energy released by the vibration day and the energy interval per unit progress are determined as the initial safety interval; the upper limit of 98.5% of the energy interval is taken as the production limit warning index value, and the lower limit of 99.7% of the energy interval is taken as the production stop warning index value. The vibration energy warning index values and disposal measures are shown in Table 4.

Table 4. Early warning index value of vibration energy and disposal measures.

Warning Level	Early Warning Item	Early Warning Energy Value	Disposal Measures
Production restriction warning	Daily energy release	18,000 J	Keep the balanced production of a single shift, organize the production according to no more than 1.5 knives per shift and no more than 4 knives per day, and maintain the advanced low stress state.
	Release energy per unit of propulsion	6000 J/m	
Stop production warning	Daily energy release	20,000 J	Stop operation on site, stop time is not less than 2 h. After the stope dynamic phenomenon is stable, the production will resume, and the production will be organized according to no more than one knife per shift and no more than three knives throughout the day until the stope energy release is stable and the state of advanced low stress is maintained.
	Release energy per unit of propulsion	7800 J/m	

6.2. Case Analysis and Verification

On 7 and 8 July 2016, there were two consecutive rockburst events in the 1300 working face and adjacent areas, of which the No. 8 event occurred in the 1301 working face. At the time of the event, the sound of dull coal cannon was heard, the shock wave was heard, coal dust was seen flying, there was low visibility, and the air volume sharply dropped (the section of the local roadway along the 1301 belt transport down chute was reduced). The location of the rockburst event is shown in Figure 18.

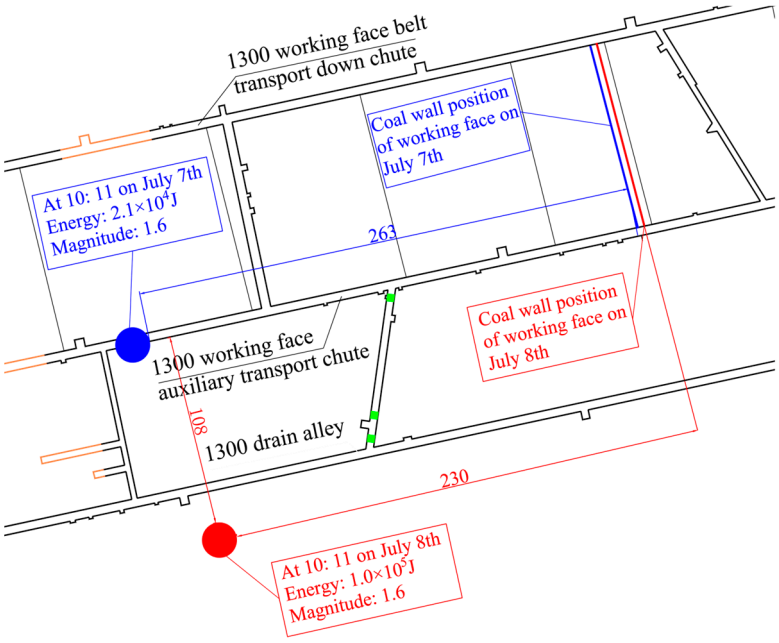

Figure 18. Location of rockburst event No.7 and No.8.

The event was accurately predicted using the micro-earthquake monitoring and warning system for rockbursts in Section 5.1. The micro-earthquake monitoring results are shown in Figure 19, which shows the frequency distribution and energy distribution of micro-earthquake events. Figure 19a shows the distribution density of microseismic events. The color of the color scale corresponds to the distribution number of different microseismic events in the corresponding area; the redder color indicates the more microseismic events. Figure 19b shows the energy distribution of microseismic events; taking lg(E), E is the total energy of all microseismic events in the region, measured in Joules. The larger the size, the more intensive the energy released by the microseismic event, and the more

serious the damage to the coal and rock mass in the region. It can be clearly seen that due to the continuous shutdown of production for many days, the bearing pressure in the surrounding rock was fully evolved. In addition to the continuous rapid progress from 5 to 8 July, on the one hand, the number of microseismic events in front of the work sharply increased; on the other hand, there were also a large number of microseismic events in the rear coal pillar area, including large energy events. However, after a recovery rate of 2.4 m/d was restored on 9 and 10 July, the microseismic events in front of the working face and coal pillar area sharply decreased, and even sporadic events occasionally occurred in the later stage. It can be inferred that the rockburst accident that occurred on 7 July and 8 August was caused by the breaking of the roof cantilever beam at the limit state, and the accident was caused by the joint action of various factors, including the continuous advance of the working face, the time production was stopped, and the speed of pushing and mining.

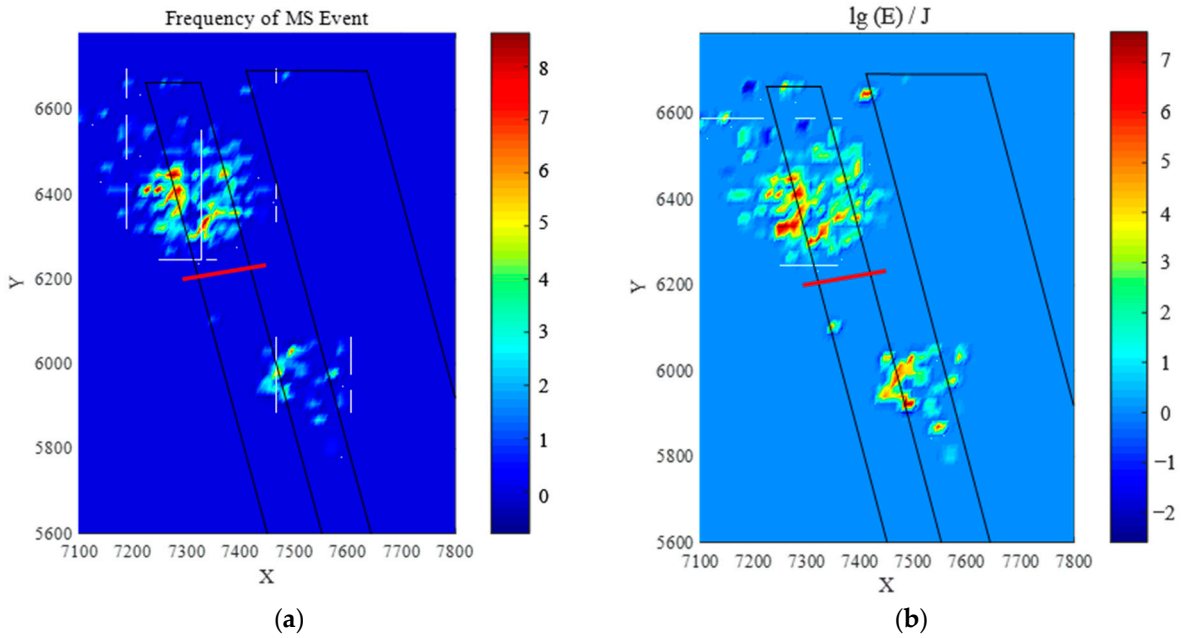

Figure 19. Energy and frequency distribution of microseismic events in July. (**a**) Frequency distribution cloud map of microseismic events. (**b**) Energy distribution cloud map of microseismic events (lg(E)).

The key measures to solve these problems are: one is to control the mining speed in the mining field. The research shows that the fundamental reason for the rockburst induced by the rapid push mining in the stope is the superposition of the advanced dynamic abutment pressure and the static abutment pressure in the stope. Under the conditions of normal speed push mining, the advance dynamic abutment pressure and static abutment pressure of the stope move forward with the roof movement, and their movement speed is essentially the same. Under the conditions of rapid push mining, with the rapid movement of low level strata, the leading dynamic bearing pressure of the stope rapidly moves forward, while the high level strata have no time to slowly move or move forward, which causes the static bearing pressure to slowly move or move forward, resulting in the superposition of the influence of dynamic bearing pressure and the influence of static bearing pressure at a certain point in advance of the stope, which may lead to rockburst [46,47]; The second measure is implement pressure relief by large diameter drilling. Large-diameter boreholes are used for pressure relief treatment in local areas with rockburst risk. Through the implementation of large-diameter drilling, the surrounding rock at a certain depth on the roadway will be structurally damaged, forming a weakening zone, causing the high stress in the surrounding rock around the roadway to be transferred deeper, so that the surrounding rock around the roadway will be in the low-stress zone. When rockbursts occur, on the one hand, the space of the large-diameter drilling can absorb the washed coal

and prevent the coal from rushing out, while on the other hand, the closure of the roof and floor in the pressure relief zone will produce a "wedge" resistance zone. This can prevent the coal body from rushing out to a certain extent [48–50].

(1) According to the previous analysis, when the daily pushing and mining speed of the 1300 working face is 4.0 m/d, rockburst will not occur. When the pushing and mining speed is 5.6 m/d, the leading dynamic abutment pressure and static abutment pressure of the stope synchronously move forward. When the pushing and mining speed is 6.4 m/d, after a period of pushing and mining, the influence of the leading dynamic abutment pressure and the static abutment pressure of the stope is superimposed, thus inducing the rockburst. It can be seen that the upper limit of mining speed can be determined by studying the evolution law of leading dynamic pressure and static abutment pressure in the stope based on the prevention and control of rockbursts.

(2) After relief treatment, such as pressure relief using large-diameter boreholes, the 1300 working face resumed production on 21 July and smoothly passed through the large fault area until the end of the mining work of the working face. The application of this technology ensures the safe production of the working face and its adjacent areas.

7. Discussion

Aimed at the problem of multiple rockburst accidents in the adjacent area of a 1300 fully mechanized caving face in a mine, this study considered the evolution and distribution laws of the surrounding rock support pressure in fully mechanized caving faces of deep well as a breakthrough point. Relying on microseismic monitoring technology, it was revealed that the cause of rockbursts in the adjacent area is actually "caused by the evolution superposition of the lateral support pressure of the 1300 stope and the original rock stress along the 1301 belt transport down chute". The supporting pressure distribution range was preliminarily obtained as 120 m. By constructing the dynamic and static support pressure calculation model of the longwall stope, with the help of CT geophysical exploration and drilling cuttings, as well as other measurement methods, it was found that the 1301 belt transport down chute is in the support pressure influence area (superposition area) of 20 m to 130 m, which further confirmed the validity of the microseismic analysis results and the accuracy of the theoretical model. Finally, combined with the field measurement results and theoretical model calculation, the corresponding rockburst early warning system and prevention measures were put forward. The research results can provide support for the early warning of mining-induced disasters in a working face. Firstly, it is beneficial for coal mining enterprises to optimize the setting of mining speed. Second, it is convenient for mining enterprises to design reasonable support and prevention strategies for rockbursts. The third is to provide theoretical support for mine safety early warnings. In addition, the results of this study not only provide a theoretical basis for the prevention and treatment of rockbursts, but also provide important reference significance for studying the inducing factors of rockbursts and improving the classification and positioning accuracy of microseismic events.

However, there are areas for improvement in this study, specifically: when calculating the theoretical model, the impact of the goaf gangue in the field was not considered. In fact, the goaf gangue affects the formation of overlying strata structures in the mining area, as well as the working conditions of the support [51]. When calculating the support pressure of the longwall mining area, various factors such as the geological profile, lithology, the mining parameters, and the gangue caving expansion coefficient need to be comprehensively considered [52]. This paper simplified the theoretical modeling process based on the main force source of rockbursts and the quantitative modeling characteristics, assuming that the content under study was under the condition of sufficient mining in the mining area, and studied the potential for rockbursts and other disaster issues in this process, ignoring the impact of the goaf gangue. In the future, we will further deepen the study of the impact of factors such as the gangue pile, and add other conditions that may affect the results of theoretical model calculation to modify the model, so as to make the obtained support pressure influence range more accurate.

8. Conclusions

Taking multiple rockburst events in the vicinity of the 1300 longwall face in a certain mine as the engineering background, the evolution and distribution characteristics of the abutment pressure in the fully mechanized caving face were obtained through field microseismic and stress measurements, and the dynamic and static abutment pressure and their calculation models were proposed, the rockburst monitoring and early warning system of the fully mechanized caving face in the deep mine was constructed, and the corresponding anti-scour engineering optimization and active weak rockburst technology were proposed. In summary, the main research conclusions are as follows:

(1) By utilizing monitoring methods, including the vibration field and stress field, the scope of mining-induced effects on the fully mechanized 1300 working face in a certain mine was determined, the evolution and distribution characteristics of the surrounding rock abutment pressure of the 1300 working face were revealed, and the distribution range of the lateral abutment pressure in the goaf was initially obtained to be 120 m (the belt transport down chute of the 1301 working face). It was revealed that the essence of the rockburst problem in the adjacent area of the fully mechanized caving face was "caused by the evolution superposition of the lateral support pressure of the 1300 stope and the original rock stress along the 1301 belt transport down chute".

(2) According to the theory of key strata, the load transfer characteristics of roof strata, and the theory of the limit equilibrium method, the calculation model of the dynamic and static abutment pressure of the longwall stope was established, and the quantitative calculation of the lateral abutment pressure of the stope was realized. It was concluded that 28 m~130 m of the 1300 goaf was the area affected by the abutment pressure, and a test of the model was realized through on-site stress detection.

(3) The internal relationship between the push mining of the fully mechanized caving face and the rockburst in the adjacent area was analyzed, the microseismic frequency, spatial distribution characteristics and the relationship between the microseismic energy release and the push mining speed were analyzed, and the microseismic response law under different push mining speeds was revealed. Based on this, the optimization design of the push mining speed was carried out;

(4) An integrated microseismic energy early warning index system for the actual mining face was established. Combined with the rockburst event on 8 July 2015, corresponding measures were proposed, including optimizing the mining speed and implementing controlled weak blasting in localized areas of the coal seam. These measures ensured the safe mining progress of the 1300 longwall face through the region and achieved secure extraction. The research outcomes of this project provide a theoretical foundation for preventing and controlling rockburst hazards, which holds significant importance for achieving safe and efficient mining in the mine.

Author Contributions: Conceptualization, Q.Z. and L.S.; methodology, L.S. and J.L.; software, Q.Z. and D.W.; validation, Y.Y., J.L. and Z.O.; formal analysis, Q.Z. and Z.O.; investigation, L.S. and D.W.; resources, Y.Y.; data curation, Z.O.; writing—original draft preparation, Q.Z., J.L. and L.S.; writing—review and editing, L.S. and D.W.; visualization, Q.Z.; supervision, Y.Y.; project administration, J.L.; funding acquisition, Q.Z. All authors have read and agreed to the published version of the manuscript.

Funding: This research was funded by the Central Guidance on Local Science and Technology Development Fund of Hebei Province, grant number 216Z5401G, S&T Program of Hebei, grant number 22375401D, the Fundamental Research Funds for the Central Universities, grant number 3142021002, and Scientific Research Program of Colleges and Universities in Hebei Province, grant number Z2020124.

Institutional Review Board Statement: Not applicable.

Informed Consent Statement: Not applicable.

Data Availability Statement: Some or all data, models or code that support the findings of this study are available from the corresponding author upon reasonable request.

Conflicts of Interest: The authors declare no conflict of interest.

References

1. Lan, T.; Fan, C.; Han, J.; Zhang, H.; Sun, J. Controlling mechanism of rock burst by CO_2 fracturing blasting based on rock burst system. *Shock Vib.* **2020**, *2020*, 8876905. [CrossRef]
2. Lyu, P.; Geng, Y. Unified Mechanism of Rock Burst Induced by Coal Mine Earthquake and Its Activity and Response Characteristics. *Shock. Vib.* **2023**, *2023*, 2145765. [CrossRef]
3. Yang, W.; Zhang, Z.; Wei, Q.; Qu, X.; Wen, J. Research on Mechanism of Rock Burst in Key Working Faces under Thick Magmatite in Deep Mine. *Shock Vib.* **2021**, *2021*, 1–17. [CrossRef]
4. Zhou, J.; Li, X.; Mitri, H. A critical survey of empirical methods for evaluating rockburst potential. In Proceedings of the 15th IACMAG, Wuhan, China, 18–22 October 2017; pp. 18–22.
5. Vu, T. Solutions to prevent face spall and roof falling in fully mechanized longwall at underground mines, Vietnam. Min. *Miner. Depos* **2022**, *16*, 127–134. [CrossRef]
6. Qiu, P.-Q.; Ning, J.-G.; Wang, J.; Hu, S.-C.; Li, Z. Mitigating rock burst hazard in deep coal mines insight from dredging concentrated stress: A case study. *Tunn. Undergr. Space Technol.* **2021**, *115*, 104060. [CrossRef]
7. Li, X.; Pan, F.; Li, H.; Zhao, M.; Ding, L.; Zhang, W. Prediction of rock-burst-threatened areas in an island coal face and its prevention: A case study. *Int. J. Min. Sci. Technol.* **2016**, *26*, 1125–1133. [CrossRef]
8. Chen, X.; Li, W.; Yan, X. Analysis on rock burst danger when fully-mechanized caving coal face passed fault with deep mining. *Saf. Sci.* **2012**, *50*, 645–648. [CrossRef]
9. Wasilewski, S. Gas-dynamic phenomena caused by rock mass tremors and rock bursts. *Int. J. Min. Sci. Technol.* **2020**, *30*, 413–420. [CrossRef]
10. Wu, M.; Ye, Y.; Wang, Q.; Hu, N. Development of rockburst research: A comprehensive review. *Appl. Sci.* **2022**, *12*, 974. [CrossRef]
11. Li, C.C.; Zhao, T.; Zhang, Y.; Wan, W. A study on the energy sources and the role of the surrounding rock mass in strain burst. *Int. J. Rock Mech. Min. Sci.* **2022**, *154*, 105114. [CrossRef]
12. Afraei, S.; Shahriar, K.; Madani, S.H. Statistical assessment of rock burst potential and contributions of considered predictor variables in the task. *Tunn. Undergr. Space Technol.* **2018**, *72*, 250–271. [CrossRef]
13. Yang, Z.; Liu, C.; Zhu, H.; Xie, F.; Dou, L.; Chen, J. Mechanism of rock burst caused by fracture of key strata during irregular working face mining and its prevention methods. *Int. J. Min. Sci. Technol.* **2019**, *29*, 889–897. [CrossRef]
14. Dychkovskyi, R.; Shavarskyi, I.; Saik, P.; Lozynskyi, V.; Falshtynskyi, V.; Cabana, E. Research into stress-strain state of the rock mass condition in the process of the operation of double-unit longwalls. *Min. Miner. Depos.* **2020**, *14*, 85–94. [CrossRef]
15. Kicki, J.; Dyczko, A. The concept of automation and monitoring of the production process in an underground mine. In *New Techniques and Technologies in Mining-Proceedings of the School of Underground Mining*; Dychkovskyy, R., Ed.; Taylor & Francis: London, UK, 2010; pp. 245–253.
16. Keneti, A.; Sainsbury, B.-A. Review of published rockburst events and their contributing factors. *Eng. Geol.* **2018**, *246*, 361–373. [CrossRef]
17. Zhu, M.; Li, B.; Liu, G. Groundwater risk assessment of abandoned mines based on pressure-state-response—The example of an abandoned mine in southwest China. *Energy Rep.* **2022**, *8*, 10728–10740. [CrossRef]
18. Tang, B.; Cheng, S.; Yeboah, M.; Cheng, H.; Tang, Y.; Wang, C. Strength of fabricated enclosed roadway support structure for TBM-excavated coal mine roadways: Experimental and numerical study. *Tunn. Undergr. Space Technol.* **2023**, *131*, 104779. [CrossRef]
19. Kang, H.; Gao, F.; Xu, G.; Ren, H. Mechanical behaviors of coal measures and ground control technology for China's deep coal mines–A review. *J. Rock Mech. Geotech. Eng.* **2022**, *15*, 37–65. [CrossRef]
20. Öge, İ.F. Revisiting the assessment of squeezing condition and energy absorption of flexible supports: A mine development case. *Tunn. Undergr. Space Technol.* **2021**, *108*, 103712. [CrossRef]
21. Islavath, S.R.; Deb, D.; Kumar, H. Development of a roof-to-floor convergence index for longwall face using combined finite element modelling and statistical approach. *Int. J. Rock Mech. Min. Sci.* **2020**, *127*, 104221. [CrossRef]
22. Pariseau, W.; Schmelter, S.; Sheik, A. Mine slope stability analysis by coupled finite element modelling. *Int. J. Rock Mech. Min. Sci.* **1997**, *34*, 242.e1–242.e17. [CrossRef]
23. Kumar, H.; Deb, D.; Chakravarty, D. Design of crown pillar thickness using finite element method and multivariate regression analysis. *Int. J. Min. Sci. Technol.* **2017**, *27*, 955–964. [CrossRef]
24. Skrzypkowski, K.; Zagórski, K.; Zagórska, A.; Apel, D.B.; Wang, J.; Xu, H.; Guo, L. Choice of the arch yielding support for the preparatory roadway located near the fault. *Energies* **2022**, *15*, 3774. [CrossRef]
25. Sakhno, I.; Sakhno, S.; Kamenets, V. Stress environment around head entries with pillarless gobside entry retaining through numerical simulation incorporating the two type of filling wallin. In *IOP Conference Series: Earth and Environmental Science*; IOP Publishing: Bristol, UK, 2022; Volume 1049, p. 012011.
26. Jing, H.; Wu, J.; Yin, Q.; Wang, K. Deformation and failure characteristics of anchorage structure of surrounding rock in deep roadway. *Int. J. Min. Sci. Technol.* **2020**, *30*, 593–604. [CrossRef]
27. Ji, S.; Wang, Z.; Karlovšek, J. Analytical study of subcritical crack growth under mode I loading to estimate the roof durability in underground excavation. *Int. J. Min. Sci. Technol.* **2022**, *32*, 375–385. [CrossRef]
28. Xu, C.; Yang, G.; Wang, K.; Fu, Q. Uneven stress and permeability variation of mining-disturbed coal seam for targeted CBM drainage: A case study in Baode coal mine, eastern Ordos Basin, China. *Fuel* **2021**, *289*, 119911. [CrossRef]

29. Guo, H.; Tang, H.; Wu, Y.; Wang, K.; Xu, C. Gas seepage in underground coal seams: Application of the equivalent scale of coal matrix-fracture structures in coal permeability measurements. *Fuel* **2021**, *288*, 119641. [CrossRef]
30. Ma, Z.; Chen, C.; Sun, X.; Wu, G.; Liu, P.; Gao, L. Test and numerical simulation of failure mechanism of barrel and wedge anchorage in coal mines. *Constr. Build. Mater.* **2020**, *237*, 117647. [CrossRef]
31. Shengrong, X.; Mingming, G.; Dongdong, C.; Yanding, S.; Hao, P.; Hai, S.; Shizhong, L. Stability influence factors analysis and construction of a deep beam anchorage structure in roadway roof. *Int. J. Min. Sci. Technol.* **2018**, *28*, 445–451. [CrossRef]
32. Zhao, Z.-G.; Zhang, Y.-J.; Li, C.; Wan, Z.; Li, Y.-N.; Wang, K.; Xu, J.-f. Monitoring of coal mine roadway roof separation based on fiber Bragg grating displacement sensors. *Int. J. Rock Mech. Min. Sci.* **2015**, *74*, 128–132. [CrossRef]
33. Rostami, J.; Kahraman, S.; Naeimipour, A.; Collins, C. Rock characterization while drilling and application of roof bolter drilling data for evaluation of ground conditions. *J. Rock Mech. Geotech. Eng.* **2015**, *7*, 273–281. [CrossRef]
34. Zhang, C.; Jin, G.; Liu, C.; Li, S.; Xue, J.; Cheng, R.; Wang, X.; Zeng, X. Prediction of rockbursts in a typical island working face of a coal mine through microseismic monitoring technology. *Tunn. Undergr. Space Technol.* **2021**, *113*, 103972. [CrossRef]
35. Zhao, J.-S.; Jiang, Q.; Lu, J.-F.; Chen, B.-R.; Pei, S.-F.; Wang, Z.-L. Rock fracturing observation based on microseismic monitoring and borehole imaging: In situ investigation in a large underground cavern under high geostress. *Tunn. Undergr. Space Technol.* **2022**, *126*, 104549. [CrossRef]
36. Ma, K.; Sun, X.; Tang, C.; Yuan, F.; Wang, S.; Chen, T. Floor water inrush analysis based on mechanical failure characters and microseismic monitoring. *Tunn. Undergr. Space Technol.* **2021**, *108*, 103698. [CrossRef]
37. Liu, C.; Li, S.; Cheng, C.; Xue, J. Activation characteristics analysis on concealed fault in the excavating coal roadway based on microseismic monitoring technique. *Int. J. Min. Sci. Technol.* **2017**, *27*, 883–887. [CrossRef]
38. Zhang, E.; Zhou, B.; Yang, L.; Li, C.; Li, P. Experimental study on the microseismic response characteristics of coal and gas outbursts. *Process Saf. Environ. Prot.* **2023**, *172*, 1058–1071. [CrossRef]
39. Barthwal, H.; van der Baan, M. Microseismicity observed in an underground mine: Source mechanisms and possible causes. *Geomech. Energy Environ.* **2020**, *22*, 100167. [CrossRef]
40. Xue, R.; Liang, Z.; Xu, N.; Dong, L. Rockburst prediction and stability analysis of the access tunnel in the main powerhouse of a hydropower station based on microseismic monitoring. *Int. J. Rock Mech. Min. Sci.* **2020**, *126*, 104174. [CrossRef]
41. Yang, C.; Luo, Z.; Hu, G.; Liu, X. Application of a microseismic monitoring system in deep mining. *J. Univ. Sci. Technol. Beijing Miner. Metall. Mater.* **2007**, *14*, 6–8. [CrossRef]
42. Shen, B.; Duan, Y.; Luo, X.; van de Werken, M.; Dlamini, B.; Chen, L.; Vardar, O.; Canbulat, I. Monitoring and modelling stress state near major geological structures in an underground coal mine for coal burst assessment. *Int. J. Rock Mech. Min. Sci.* **2020**, *129*, 104294. [CrossRef]
43. Jinqiang, W.; Basnet, P.; Mahtab, S. Review of machine learning and deep learning application in mine microseismic event classification. *Min. Miner. Depos.* **2021**, *15*, 19–26. [CrossRef]
44. Duan, Y.; Shen, Y.; Canbulat, I.; Luo, X.; Si, G. Classification of clustered microseismic events in a coal mine using machine learning. *J. Rock Mech. Geotech. Eng.* **2021**, *13*, 1256–1273. [CrossRef]
45. Liu, J.; Jiang, F.; Zhu, S. Study of dynamic and static abutment pressure around longwall face and its application. *Chin. J. Rock Mech. Eng.* **2015**, *34*, 1815–1827.
46. Wang, C.; Si, G.; Zhang, C.; Cao, A.; Canbulat, I. Variation of seismicity using reinforced seismic data for coal burst risk assessment in underground mines. *Int. J. Rock Mech. Min. Sci.* **2023**, *165*, 105363. [CrossRef]
47. Li, X.; Chai, Y. Determination of pillar width to improve mining safety in a deep burst-prone coal mine. *Saf. Sci.* **2019**, *113*, 244–256. [CrossRef]
48. Song, D.; Wang, E.; Liu, Z.; Liu, X.; Shen, R. Numerical simulation of rock-burst relief and prevention by water-jet cutting. *Int. J. Rock Mech. Min. Sci.* **2014**, *70*, 318–331. [CrossRef]
49. He, S.; Song, D.; He, X.; Chen, J.; Ren, T.; Li, Z.; Qiu, L. Coupled mechanism of compression and prying-induced rock burst in steeply inclined coal seams and principles for its prevention. *Tunn. Undergr. Space Technol.* **2020**, *98*, 103327. [CrossRef]
50. Chen, X.; Li, L.; Wang, L.; Qi, L. The current situation and prevention and control countermeasures for typical dynamic disasters in kilometer-deep mines in China. *Saf. Sci.* **2019**, *115*, 229–236. [CrossRef]
51. Malashkevych, D.; Petlovanyi, M.; Sai, K.; Zubko, S. Research into the coal quality with a new selective mining technology of the waste rock accumulation in the mined-out area. *Min. Miner. Depos* **2022**, *16*, 103–114. [CrossRef]
52. Smoliński, A.; Malashkevych, D.; Petlovanyi, M.; Rysbekov, K.; Lozynskyi, V.; Sai, K. Research into Impact of Leaving Waste Rocks in the Mined-Out Space on the Geomechanical State of the Rock Mass Surrounding the Longwall Face. *Energies* **2022**, *15*, 9522. [CrossRef]